HHS Public Access

Author manuscript

Cell Rep. Author manuscript; available in PMC 2023 March 20.

Published in final edited form as:

Cell Rep. 2022 March 08; 38(10): 110473. doi:10.1016/j.celrep.2022.110473.

Deletion of STAT3 from Foxd1 cell population protects mice from kidney fibrosis by inhibiting pericytes trans-differentiation and migration

Amrendra K. Ajay[1,*], **Li Zhao**[1], **Shruti Vig**[1], **Mai Fujikawa**[2], **Sudhir Thakurela**[3], **Shreyas Jadhav**[1], **Andrew Cho**[1], **I-Jen Chiu**[1], **Yan Ding**[1], **Krithika Ramachandran**[1], **Arushi Mithal**[1], **Aanal Bhatt**[1], **Pratyusha Chaluvadi**[1], **Manoj K. Gupta**[4], **Sujal I. Shah**[5], **Venkata S. Sabbisetti**[1], **Ana Maria Waaga-Gasser**[1], **David A. Frank**[6,7], **Gopal Murugaiyan**[2], **Joseph V. Bonventre**[1], **Li-Li Hsiao**[1,*]

[1]Division of Renal Medicine, Department of Medicine, Brigham and Women's Hospital and Harvard Medical School, Boston, MA, USA, 02115.

[2]Ann Romney Centre for Neurological Disease, Department of Neurology, Brigham and Women's Hospital and Harvard Medical School, Boston, MA, USA, 02115.

[3]Broad Institute of MIT and Harvard, Cambridge, MA, USA, 02142. Department of Stem Cell and Regenerative Biology, Harvard University, Cambridge, MA, USA, 02138.

[4]Section of Islet Cell Biology and Regenerative Medicine, Joslin Diabetes Center and Harvard Medical School, Boston, MA, USA, 02215.

[5]Department of Pathology, Brigham and Women's Hospital and Harvard Medical School, Boston, MA, USA, 02115.

[6]Department of Medical Oncology, Dana Farber Cancer Research Institute, Boston, MA, USA, 02215.

[7]Department of Medicine, Brigham and Women's Hospital, and Harvard Medical School, Boston, MA, USA, 02115.

SUMMARY

STAT3 is a key transcription factor implicated in the pathogenesis of kidney fibrosis. Although, *Stat3* deletion in tubular epithelial cells is known to protect mice from fibrosis, the exact function of STAT3 in Foxd1 cells remains unknown. Here, using Foxd1-mediated *Stat3* knock-out

[*]**Corresponding authors:** Amrendra K. Ajay, Ph.D. Division of Renal Medicine, Department of Medicine, Brigham and Women's Hospital, Harvard Medical School. 221 Longwood Ave BLI, 447A, Boston, MA 02115. Phone: (617) 525-7414; Fax: (617) 525-7386; akajay@bwh.harvard.edu, Dr. Li-Li Hsiao, M.D., Ph.D., Division of Renal Medicine, Department of Medicine, Brigham and Women's Hospital, Harvard Medical School., 221 Longwood Ave BLI, 449C, Boston, MA 02115., Phone: (617) 525-7366; Fax: (617) 525-7386; lhsiao@bwh.harvard.edu.
Lead contact: Amrendra K. Ajay, akajay@bwh.harvard.edu

AUTHOR CONTRIBUTIONS

Conceptualization, A.A., V.S., A.W., G.M., D.F., J.B. and LL.H.; Data curation, A.A., L.Z., S.V., M.F., K.R., P.C., A.M., A.B., M.K., S.T., A.C., S.S.; Investigation, A.A., L.Z., S.V.; Visualization, A.A., S.V., M.F., G.M., S.T.; Methodology, A.A., L.Z., S.V., G.M., S.J., I.JC., K.R., S.T., V.S.; Writing, A.A. and LL.H., Review and editing, all authors; Funding acquisition, A.A., V.S., J.B., LL.H.

COMPETING INTERESTS STATEMENT

The authors declare no competing interests.

mice, CRISPR and inhibitors of STAT3 we investigate its function. STAT3 is phosphorylated in tubular-epithelial-cells in acute kidney injury whereas it is expanded to interstitial cells in fibrosis in mice and humans. Foxd1-mediated deletion of *Stat3* protects mice from folic acid- and aristolochic acid-induced kidney fibrosis. Mechanistically, STAT3 upregulates the inflammation and differentiates pericytes into myofibroblasts. STAT3 activation increases migration and profibrotic signaling in genome-edited pericyte-like cells. Conversely, blocking *Stat3* inhibits detachment, migration, and profibrotic signaling. Furthermore, STAT3 binds to the *Collagen1a1* promoter in mouse kidneys and cells. Together, our study identifies a previously unknown function of STAT3 that promotes kidney fibrosis and have therapeutic value in fibrosis.

Graphical Abstract

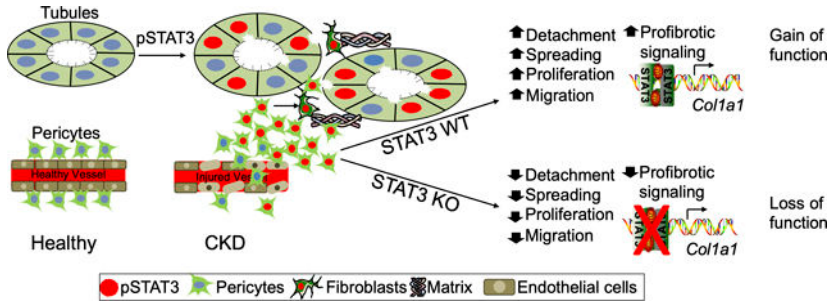

Keywords

STAT3; fibrosis; inflammation; stromal cells; pericytes; myofibroblasts transformation

INTRODUCTION

Diverse cell types play crucial functions in the cellular processes of tissue fibrosis, (Quan et al., 2006; Willis et al., 2006; Wynn, 2007; Zeisberg et al., 2007) including kidney fibrosis (E and Humphreys, 2017; El Agha et al., 2017; Kramann et al., 2015b; Mack and Yanagita, 2015). Although many cell types in the tubulo-interstitium of the kidneys produce extracellular matrix (ECM), with fibroblasts being the principal cells, the contribution of other cell types are not well understood. Recent reports indicate that pericytes are a critical source of myofibroblasts in fibrotic kidneys (Duffield and Humphreys, 2011; Humphreys et al., 2010; Lin et al., 2008; Schrimpf and Duffield, 2011). Following kidney injury, pericytes detach from the endothelium proliferate, migrate, and transdifferentiate into myofibroblasts (Humphreys et al., 2010; Lin et al., 2008).

Signal Transduction and Activator of Transcription 3 (STAT3) is phosphorylated in multiple cell types including fibroblasts, immune cells, and epithelial cells in response to growth factors and inflammatory response (Leu et al., 2003; Okamoto et al., 1997). TGF-β dependent STAT3 activation (Zehender et al., 2018) increases the profibrotic signaling in fibroblasts in systemic sclerosis (Chakraborty et al., 2017). Depending on the type of growth factor and cellular machinery, STAT3 initiates specific transcriptional programs in the cells (Kasembeli et al., 2018; Shain et al., 2009; Yu et al., 2009). STAT3 deletion from macrophages and cardiomyocytes increases skin and cardiac fibrosis in mice (Do

et al., 2018; Jacoby et al., 2003). STAT3 inhibition by its small molecule inhibitor, S3I-201 or stattic, protects mice from kidney fibrosis and Autosomal Dominant Polycystic Kidney Disease (Pang et al., 2010; Takakura et al., 2011). Furthermore, genetic depletion of STAT3 from tubular epithelial cells protects mice from nephrectomy-induced kidney fibrosis by inhibiting tubulo-interstitial crosstalk (Bienaime et al., 2016). STAT3 deletion from podocytes protects mice from HIV-1-associated nephropathy (Gu et al., 2013). We and others have shown that STAT3 regulates the expression of Kidney Injury Molecule-1 (KIM-1) following acute kidney injury (Ajay et al., 2014b; Collier and Schnellmann, 2017) and fibrinogen gamma chain in fibrotic kidneys (Craciun et al., 2014). Furthermore, we found that IL-6 mediates STAT3 phosphorylation in human proximal tubular epithelial cells in acute kidney injury (AKI) (Ajay et al., 2014b) and IL-6-mediated STAT3 activation is observed in fibroblasts *in vitro* (Craciun et al., 2014). In summary, it appears that STAT3 affects multiple cell types involved in fibrosis. However, the role of STAT3 in the stromal cells, particularly in pericytes, in kidney fibrosis remains unknown. Thus, investigating the role of STAT3 in pericytes may provide better understanding of the mechanism of kidney fibrosis, which may offer novel therapeutic targets.

In the present study, we found that *Stat3* KO from Foxd1 cell population protects from folic acid- and aristolochic acid-induced kidney fibrosis. Our gain-of-function and loss-of-function studies revealed that STAT3 directly regulates the inflammatory pathway, DNA damage, and proliferation, migration, and differentiation of pericytes into myofibroblasts. Furthermore, we found that STAT3 binds to the promoter of *Collagen1a1* gene to execute the fibrotic process. Together, our study defines a previously unknown function by which STAT3 in Foxd1 cell population promotes kidney fibrosis.

RESULTS

STAT3 expression is increased in AKI and CKD in human and mouse kidneys

We obtained human kidney specimens from the Brigham and Women's Hospital pathology core from healthy individuals, those with Acute Tubular Necrosis (ATN) representing AKI, and Diabetic Nephropathy (DN) representing CKD. We found that phosphorylation of STAT3 is increased in AKI and CKD kidneys when compared to healthy kidneys. In humans, pSTAT3 expression is limited to the tubular epithelial cells of patients with ATN, while pSTAT3 was found in both tubular epithelial and interstitial cells of the patients with CKD (Figure 1A). Of note, the total number of tubular epithelial cells in both AKI and CKD were marginally decreased but the number of interstitial cells were significantly increased in CKD (Figures S1A and S1B). Moreover, our immunostaining results showed increased expression of STAT3 in the kidneys of CKD patients (Figure 1B). Furthermore, to investigate the identity of interstitial cells expressing pSTAT3, we co-immunostained them with myofibroblast marker α-SMA and found that pSTAT3 is significantly increased in the myofibroblasts (Figure 1C). Analogous to those in humans, mouse kidneys with Folic Acid (FA)- or Aristolochic Acid (AA)-induced injury also showed increased STAT3 phosphorylation. Specifically, we found increased pSTAT3 in tubular epithelial cells in AKI (2-days post-FA treatment) and in interstitial cells in fibrotic kidneys (14-days post-FA treatment) when compared to those without FA treatment (Figure 1D). Next, we performed

western blot analysis of pSTAT3 in kidney tissues from mice with or without AKI, and kidney fibrosis and found that significantly increased pSTAT3 in AKI (2-days post-FA or 4-days post-AA treatments) and fibrotic kidneys (14-days post-FA or AA treatment) when compared to those without FA or AA treatment (Figures 1E and 1F).

In addition, we found that interstitial myofibroblasts, which are known to play important roles in fibrosis, were positive for pSTAT3 as demonstrated by co-expression of a myofibroblast marker, α-SMA, 14-days post-FA treatment (Figure 1D). Furthermore, we investigated the pSTAT3-positive cell types within the interstitium and found that in addition to myofibroblasts, pericytes also have increased pSTAT3, as shown by co-immunostaining for either NG2 or PDGFRβ in AA-induced fibrotic kidneys (Figures 1G and 1H) at 14-days post-AA treatment, as compared to normal kidneys. In accordance with FA-induced fibrosis (Figure 1D), α-SMA was increased 14-days post-AA treatment as compared to day 0 (Figure 1I).

Stromal cell-specific deletion of *Stat3* protects mice from kidney fibrosis

A previous study showed that *Stat3* deletion from tubular epithelial cells protects mice from kidney fibrosis (Bienaime et al., 2016). We aimed to investigate the functions of STAT3 activation in the stromal cells, a cell population known to differentiate into myofibroblasts. To this aim, we developed a Foxd1 cell population-specific (stromal and glomerular cells) *Stat3* deficient mice by crossing $Stat3^{flox/flox}$ mice and $Foxd1^{GC}$ mice (Figures S2A, S2B and S2C). To confirm that the pSTAT3 expression was decreased in pericytes, we performed co-immunostaining of pSTAT3 with NG2 and found decreased numbers of pSTAT3 and NG2 double-positive cells in *Stat3* KO mice as compared to control mice at 14-days post-AA treatment (Figure S2D). Furthermore, we performed qRT-PCR analysis of STAT3 mRNA in isolated primary pericytes from control and *Stat3* KO mice at 14-days post-AA treatment and found a significant decrease in *Stat3* mRNA in *Stat3* KO mice (Figure S2E).

Next, we investigated the kidney function in these mice following FA- or AA-induced AKI and fibrosis. We did not find any significant difference in BUN and sCr in AKI (post-FA treatment Figures 2A and 2B nor 4-days post-AA treatment Figures 2C and 2D) between control ($Stat3^{fl/fl}$) and *Stat3* KO ($Foxd1^{GC}$ $Stat3^{fl/fl}$) mice. Furthermore, our results show similar tubular injury in the AKI phase for both control and *Stat3* KO mice (Figures S3A and S3D); these observations were confirmed by mRNA levels of *Tnfa* and proximal tubular epithelial cell injury marker, *Hacvr1,* suggesting that *Stat3* deletion in stromal cells did not affect the intensity of AKI (Figures S3B, S3C, S3E and S3F).

We then assessed the functional roles of STAT3 in the fibrotic models using FA- or AA-treated mice for 7 days and 14 days. While our results revealed no significant difference in kidney function as assessed by BUN and sCr between control and *Stat3* KO mice in FA-treated groups, we found that the *Stat3* KO group had better kidney function in AA-treated mice (Figures 2A–2D). We then evaluated the extent of kidney injury by assessing the degree of fibrosis, myofibroblast activation, and tubular damage in both FA- and AA-treatment groups. Using MTS staining, we found a significant decrease in fibrosis in *Stat3* KO mice as compared to control mice (Figures 2E and 2F; Figures S4A and S4B (low magnification)). Myofibroblast activation, assessed by α-SMA staining, a cellular

marker of myofibroblast, was also decreased in *Stat3* KO mice (Figures 2G and 2H). We further assessed the tubular function by staining for Lotus Tetragonolobus Lectin (LTL), which binds to the the fucosyl oligosaccharides present on the brush borders of the healthy proximal tubular cells. LTL staining showed preservation of the proximal tubule brush border in *Stat3* KO mouse kidneys 14-days post-AA treatment (Figures 2G and 2H). In addition, we found a decrease in the expressions of *Collagen1a1, Fibronectin1,* and *Acta2* in *Stat3* KO mice when compared with control mice (Figures 2I–2K and 2M–2O) in both FA- and AA-induced fibrotic kidneys. Furthermore, we found decreased gene expression of *Havcr1* in *Stat3* KO mice as compared to control mice (Figures 2L and 2P) in both FA- and AA-induced fibrotic kidneys. Taken together, these data confirm that *Stat3* KO mice are protected from kidney fibrosis and tubular injury. As Foxd1 is also expressed by glomerular cells, including podocytes, we next investigated the glomerular phenotype in the *Stat3* KO mice following AA-induced fibrosis at day 14. We found *Stat3* KO mice were protected from glomerular injury as assessed by increase in glomerular size (Figure 2Q). Next, we immunostained the glomerulus with podocyte markers, podocin and synaptopodin, which showed increased coverage in Stat3 KO mice (Figures 2R and 2S), indicating preservation of podocytes compared to control mice. Finally, immunostaining of α-SMA showed increased myofibroblasts in and around the glomerulus, indicating glomerular injury/sclerosis (Figure 2S). Together, our results indicate that *Stat3* depletion from stromal cells has protective effects on kidney fibrosis in FA- and AA-induced mouse models.

Foxd1 lineage specific *Stat3* deletion results in reduced inflammation, DNA damage, and cell proliferation in the fibrotic kidneys, *in vivo*

To understand the mechanisms by which Foxd1 lineage specific deletion of *Stat3* protects mice from kidney fibrosis, we investigated the involvement of inflammatory pathways in the pericytes and macrophages of AA-induced kidney fibrosis model. We found that infiltration of macrophages (stained by F4/80, a cellular marker of macrophages) in the kidney was significantly reduced in *Stat3* KO as compared to control mice (Figure 3A). We then isolated the macrophages from control and *Stat3* KO fibrotic mouse kidneys using F4/80 and CD11b markers and found a decrease in number of macrophages in *Stat3* KO mouse kidneys as compared to control kidneys (Figure 3B). Furthermore, gene expressions of inflammatory mediators *Il1b*, *Il6*, *Il12*, *Il23*, *Ifng*, *Nos2,* and *Tnfa* were decreased in the macrophages of *Stat3* KO mice as compared to control mice at day 14-post AA treatment (Figure 3C). On the other hand, expression levels of M2 macrophages markers *Il10, Tgfb*, *Arg1, Mrc1, Retnla, and Chil3,* were increased in the *Stat3* KO mice as compared to control mice at day 14-post-AA treatment (Figure 3D). Further, to investigate whether macrophages play important role in resolution of injury by switching into M1 (inflammatory) or M2 (reparative) subtypes, we performed co-immunostaining for F4/80 and IL10. We found a significant increase in IL-10 staining in *Stat3* KO mice as compared to control mice at 14-days post-AA treatment (Figure 3E).

Additionally, to assess the involvement of STAT3 in DNA damage signaling and in the proliferation of tubular and interstitial cells, we stained for pH2AX and Ki67, respectively. We found that *Stat3* KO mice show reduced DNA damage of both interstitial and tubular epithelial cells (Figure 3F). Further, to investigate the identity of interstitial

pH2AX-expressing cells in the control mice at 14-days post-AA treatment, we performed co-immunostaining with PDGFRβ and found a significant number of double-positive cells, indicating the stromal cell origin (Figure 3G).

We also found decreased numbers of interstitial and tubular Ki67-positive cells in *Stat3* KO mice (Figure 3H). Finally, to investigate the identity of interstitial Ki67-expressing cells in the control mice at 14-days post-AA treatment, we performed co-immunostaining with PDGFRβ and found a significant number of double-positive cells, indicating the stromal cell lineage (Figure 3I). Taken together, our results indicate that the depletion of *Stat3* from Foxd1 lineage protects mice from kidney fibrosis by reducing inflammation, DNA damage, and proliferation of the interstitial cells by increasing the polarization of M2 macrophages.

IL-6-mediated STAT3 phosphorylation leads to increased proliferation, migration, and profibrotic signaling in pericyte-like 10T1/2 cells, *in vitro*

It has been shown that stromal cells, including pericytes, can differentiate into myofibroblasts (Humphreys et al., 2010; Kida and Duffield, 2011; Kramann and Humphreys, 2014; Wang et al., 2017; Wu et al., 2013). Due to the lack of a pericyte cell line, we utilized 10T1/2 cells of mesenchymal stem cell origin, which are widely used for studying pericyte biology in various organs including the kidney (Artaza et al., 2008; DiRocco et al., 2013; Fabian et al., 2012). Because an increase in IL-6 has been reported in the pathogenesis of kidney disease, (Chen et al., 2020b; Ding et al., 2020; Magno et al., 2019) we explored its function in STAT3-mediated proliferation, migration, and induction of fibrotic signaling in 10T1/2 cells. We found that pSTAT3 is increased and translocated to the nucleus after IL-6 treatment, and that was inhibited by stattic, a specific inhibitor of STAT3, indicating that these cells responded to IL-6 (Figures 4A and 4B). We also found increased proliferation of 10T1/2 cells after IL-6-induced STAT3 activation, which was also inhibited by stattic as shown by BrdU incorporation and Ki67 staining (Figures 4C–4E). Migration of pericytes to the site of injury is one of the critical steps for the development of fibrosis (Lin et al., 2011; Lin et al., 2008). We found that an increase in the migration of 10T1/2 cells was associated with the phosphorylation of STAT3, as shown by scratch assay and transwell migration assay; this process can likewise be inhibited by stattic (Figures 4F and 4G; Figure S4C). We also report here that the phosphorylation of STAT3 increased the phosphorylation and nuclear translocation of profibrotic transcription factor SMAD2, which was also inhibited by stattic (Figure 4H). In addition, increased STAT3 phosphorylation by IL-6 resulted in higher levels of the fibrotic markers Collagen1, Fibronectin, and α-SMA (Figures 4I–4K). Interestingly, stattic effectively inhibited IL-6-induced upregulation of these fibrotic markers. Thus, these data indicate that IL-6-mediated STAT3 phosphorylation increases proliferation, migration, and profibrotic signaling in 10T1/2 cells.

STAT3 directly regulates proliferation, migration, and profibrotic signaling in pericytes, *in vitro*

To investigate the function of STAT3 phosphorylation in pericytes, we established cellular models for gain and loss of STAT3 function. We generated CRISPR-mediated STAT3 Synergistic Activation Mediator (SAM), which transcriptionally activates STAT3 expression as well as STAT3-C by mutating Alanine 662 and Asparagine 664 to Cystines and leads to

dimerization and constitutive activation of STAT3 (Figure 5A). SAM STAT3 and STAT3-C cells showed abundance of pSTAT3 as compared to control cells (Figure 5B). Furthermore, we found that the expression of profibrotic transcription factor pSMAD2 and fibrotic markers Collagen1, Fibronectin, and α-SMA was increased in STAT3-activated cells as compared to control cells (Figures 5C–5F). In addition, we tested the function of STAT3 in the migration of 10T1/2 cells. STAT3-activated cells (SAM STAT3 and STAT3-C) showed increased transwell migration with increased cell area as compared to control cells (Figure 5G).

We then investigated whether STAT3 played direct roles in cell proliferation, cell detachment, cell spreading, and cell migration. To investigate these phenotypes, we knocked out *Stat3* in 10T1/2 using CRISPR as a loss-of-function model. *Stat3* KO cells showed genomic deletion and absence of STAT3 protein as compared to *Stat3* WT cells (Figure S5). Our results demonstrated that *Stat3* KO cells exhibited decreased proliferation, surface attachment, spreading, and migration as compared to *Stat3* WT cells (Figures 5H–5K). We next examined pericytes from fibrotic kidneys of control and *Stat3* KO mice. For this, we isolated pericytes via FACS-sorting using NG2, CD140b-positive, and CD31-negative markers as shown in Figure 5L. Interestingly, we found that the gene expressions of the fibrotic factors including *Acta2*, *Col1a1*, *Fn1, Tgfb1*, and *Tgfbr1* were decreased in *Stat3* KO pericytes (Figure 5M). Taken together, these data indicate that STAT3 plays a direct role in regulating proliferation, cell detachment, cell spreading, cell migration, and profibrotic signaling of pericytes, leading to the development of fibrosis.

STAT3 transcriptionally promotes *Collagen1a1* gene expression to execute fibrotic signaling *in vivo* and *in vitro*

To further probe how STAT3 regulates profibrotic signaling, we performed in silico analysis of promoter binding on the *Collagen1a1* promoter. It was predicted that human and mouse *Collagen1a1* promoters contain consensus sequence for STAT3 binding (Figure S6). Furthermore, we used STAT3 ChIP-seq data from mouse kidney tissues (Lee et al., 2018). Re-analysis of ChIP sequencing data from WT kidneys shows that STAT3 binds the *Collagen1a1* promoter but not the *Fibronectin1* promoter (Figures 6A and 6B). To confirm the binding of STAT3 on the promoter of the *Collagen1a1* gene, we performed ChIP assay in mouse kidneys and found that STAT3 binding was increased at day 14 post-AA as compared to mice without AA treatment (Figure 6C). Moreover, we found a significant increase in the binding of STAT3 on the *Collagen1a1* promoter in our STAT3 gain-of-function pericytes cells as compared to control cells (Figure 6D). We then assessed the STAT3 transactivation in gain and loss-of-function pericytes cell models, using luciferase assay. We found a significant increase in luciferase activity in STAT3 gain-of-function models, while a significant decrease was seen in loss-of-function models as compared to the respective control cells (Figures 6E and 6F). Thus, these data indicate that STAT3 directly regulates a key pro-fibrotic factor, *Collagen1a1*, by binding to its promoter *in vivo* and *in vitro*.

DISCUSSION

Kidney fibrosis affects 10–15 % of the population in the USA (Centers for Disease and Prevention, 2007; Coresh et al., 2003; Coresh et al., 2005; Coresh et al., 2007). The functions of various cell types and their involvement has been documented but till now, the function of the pericyte and their signaling pathway in tissue fibrosis remains poorly studied. Recent studies using mouse models of kidney, heart, and liver fibrosis by Kramann *et. al.* showed that sonic hedgehog-mediated activation of Gli pathways control fibrosis development (Kramann et al., 2015a; Kramann et al., 2015b). Differentiation of various cell types into myofibroblasts has been an active area of research in the field of kidney fibrosis but the exact mediators of cell differentiation are not well understood. Apart from the Gli pathways, the most extensively studied pathways are the TGF-β (Chen et al., 2012; Lin et al., 2005; Sato et al., 2003), Wnt1 (Happe et al., 2009; He et al., 2009), and hippo signaling (Anorga et al., 2018; Seo et al., 2016) pathways. Blocking TGF-β1 and β-Catenin crosstalk exacerbates CKD (Nlandu-Khodo et al., 2017). Deletion of TGF-β receptor from kidney collecting system exacerbates fibrosis (Gewin et al., 2010), whereas TGF-β is also known to promote fibrosis by enhancing macrophage infiltration or converting of pericytes into myofibroblasts (Chung et al., 2018; Wu et al., 2013). These data make TGF-β a difficult therapeutic target.

Activation of Wnt signaling, induced by either TGF-β or other signaling pathways, promotes fibrosis (Zhang et al., 2012). But the role of Wnt signaling remains unclear in kidney repair and fibrosis (Gewin, 2018). Reports show that systemic inhibition of Wnt/β-catenin protects mice from kidney fibrosis (Hao et al., 2011; Madan et al., 2016; Surendran et al., 2005; Xiao et al., 2016; Zhou et al., 2015). On the other hand, inhibition of β-catenin showed enhanced survival of fibroblasts and increased fibrosis in mice. This confirms opposing functions of β-catenin in kidney fibrosis (Maarouf et al., 2016; Nlandu-Khodo et al., 2017; Zhou et al., 2013).

Hippo signaling plays an important role in the promotion of CKD. Activation of Yes-Associated protein (YAP) in kidney tubular cells enhances diabetic kidney disease in mice (Chen et al., 2020a; Patel et al., 2019; Seo et al., 2016). In contrast, the EGF-mediated activation of YAP plays a crucial role in recovery from AKI (Chen et al., 2018). There is significant cross talk among these three major pathways in organ fibrosis. Thus, there is a need to design a specific therapeutic regimen (Piersma et al., 2015). Therapeutic efficacy in animal models shows promising results for these three major pathways, but clinical trials often fail due to adverse effects. Thus, novel therapeutic targets are needed to alleviate kidney disease.

The origin of myofibroblasts in kidney fibrosis has been controversial. Whereas one group supports the hypothesis that neither PDGFRβ-positive nor NG2-positive cells contribute to the myofibroblast pool in development of kidney fibrosis (LeBleu et al., 2013), another group demonstrated that PDGFRβ-positive cells do indeed contribute to the myofibroblast pool in kidney, lung, and heart fibrosis (Henderson et al., 2013). Our data supports the hypothesis that PDGFRβ-positive and NG2-positive pericytes detach from the endothelium and acquire a myofibroblastic phenotype. The PDGFRβ-positive myofibroblasts have been

repeatedly described (Asada et al., 2011; Humphreys et al., 2010; Kramann et al., 2013) but recent studies using *in vivo* genetic lineage tracing methods indicate that all myofibroblasts express PDGFRβ and that Gli1-positive cells do not acquire significant NG2 expression in fibrosis models (Kramann et al., 2015b).

Understanding the cellular and molecular signaling of the cell types involved in the progression of kidney fibrosis is an important step towards the development of anti-fibrotic therapeutic strategies. STAT3 signaling has been implicated in organ fibrosis including kidney fibrosis (Bienaime et al., 2016; Kasembeli et al., 2018), where genetic ablation of *Stat3* from tubular epithelial cells protects mice from 5/6 nephrectomy-induced kidney fibrosis by disrupting tubulointerstitial communication (Bienaime et al., 2016). In this previous report, tubular cell function of STAT3 was well-documented, however, the function of stromal cells remains unknown. Our data shows that STAT3 in the Foxd1 lineage is crucial for the development of kidney fibrosis and that genetic deletion of *Stat3* from Foxd1-positive cells protect mice from kidney fibrosis. Although delineating the quantitative contribution of specific cell sub-types from the stromal cells is needed to confirm the extent of protection, our results indicate 50% protection after *Stat3* deletion using fibrotic assays such as IFTA scoring and semi-quantitative analyses of *Fibronectin1*, *Collagen1a1,* and *Acta2* in two mechanistically different mouse models of kidney fibrosis. Further, we found that *Stat3* deletion shows preservation of podocytes as well as protection from glomerular injury. In addition to the mouse data, we found that STAT3 phosphorylation is significantly increased in interstitial cells of CKD patients. These findings are particularly important for the translational potential of STAT3 inhibition in patients with CKD.

We found that both total and phospho-STAT3 is increased in both FA and AA-induced kidney fibrosis. The increase in STAT3 activation could be caused by increased levels of total STAT3 as well as by an increase in STAT3 activating stimuli such as IL-6 during kidney fibrosis. In fact, previous studies have shown IL-6 is increased in patients with CKD and its mouse models (Dalla Vestra et al., 2005; Navarro et al., 2006). It has been reported that STAT3 promoter contains IL-6 response element, a low affinity STAT3-binding element and a cAMP-responsive element (CRE). STAT3 transcription occurs in cooperation with CRE-binding protein (Ichiba et al., 1998; Narimatsu et al., 2001). Furthermore, estrogen has been shown to induce the accumulation of Estrogen Receptor α (Erα) on STAT3 promoter which leads to the expression of STAT3 (Gao et al., 2006). β-catenin also enhances both STAT3 mRNA and protein levels by binding to TCF element present in the STAT3 promoter (Yan et al., 2008). Many of these pathways are significantly upregulated in kidney fibrosis (Navarro et al., 2006; Xiao et al., 2016) and thus, STAT3 transcription may occur though one or more of these pathways. These findings are consistent with our previous findings as well as reports from other laboratory showing that STAT3 expression changes following kidney injury (Craciun et al., 2014), (Ajay et al., 2014b; Liu et al., 2012; Pang et al., 2010).

Initiation of fibrosis is orchestrated by sequential activation of various cell types and one of the most common prominent pathways is inflammation. We and others have shown that DNA damage in AKI generates Reactive Oxygen Species (ROS), which triggers DNA damage signaling and activation of STAT3 pathways. In fact, STAT3 upregulation is associated with development of AKI (Dube et al., 2017; Nechemia-Arbely et al., 2008)

and fibrosis (Ajay et al., 2014a; Craciun et al., 2014; Pace et al., 2019; Pang et al., 2010). Persistent inflammation of tubules or interstitium initiates the progression of fibrosis. However, the function of STAT3 in pericytes and its function/role in DNA damage and inflammation remains unclear. Our data show that *Stat3* depletion from Foxd1 lineage limits macrophage infiltration, restricts its inflammatory capabilities, and promotes M2 polarization, which helps to resolve inflammation. In accordance with these data, we found that *Stat3* depletion reduced DNA damage signaling and decreased proliferation of tubular epithelial cells and interstitial cells in the fibrotic kidneys of *Stat3* KO mice.

Myofibroblasts, a cell type that is well-studied to lay matrix leading to fibrosis in chronic kidney disease, are differentiated from different cell types, pericytes being one of them (Campanholle et al., 2013; Kramann et al., 2013; LeBleu et al., 2013). How pericytes differentiate into myofibroblasts is not well understood. We found that STAT3 is phosphorylated in tubular epithelial cells as well as in interstitial cells in human CKD kidneys and experimental mouse models of kidney fibrosis. Our data show that *Stat3* KO in Foxd1 lineage protects mice from FA- or AA-induced kidney fibrosis. Multiple models used in our study to increase STAT3 activation, including IL-6-mediated increase and CRISPR-mediated transcriptional as well as mutation-induced gain-of-function, all show that STAT3 is involved in proliferation, migration, and increase in profibrotic signaling in pericyte-like cells. We found a significant increase in profibrotic signaling in STAT-C cells as compared to SAM STAT3 cells, which positively correlates with the amount of nuclear STAT3. These data confirm that STAT3 phosphorylation and its nuclear translocation directly regulate profibrotic signaling in pericyte-like cells. Stattic, a specific small molecular inhibitor of STAT3, inhibited IL-6-mediated proliferation, migration, and profibrotic signaling, and *Stat3* KO from the pericyte-like cells reduced the detachment, spreading, proliferation, and migration of these cells. Furthermore, pericytes isolated from *Stat3* KO fibrotic mouse kidneys showed decreased expression of profibrotic signaling molecules *Fibronectin1*, *Collagen1a1,* and *Acta2*. Together, these data confirm a crucial function of STAT3 in the pericytes.

Binding of STAT3 on specific gene promoters decide the outcome of the cellular phenotype. For instance, STAT3 binding on *OCT4* and *NANOG* gene promoters regulates stem cell proliferation (Do et al., 2013), STAT3 binding on promoters of *Cyclin D1* and *c-MYC* causes cancer cell proliferation, controls the cell cycle, and deposits extracellular matrix (Zhang et al., 2003), and binding of STAT3 on *Havcr1* promoter leads to tubular cell damage through activation of DNA damage-induced inflammation (Ajay et al., 2014a; Collier and Schnellmann, 2017). Previously, we have shown that STAT3 binds on promoters of *Havcr1* and *fibrinogen* α, β as well as γ genes in AKI and fibrotic kidneys respectively (Ajay et al., 2014a; Craciun et al., 2014). Here, we found that STAT3 binds on the promoter of *Collagen1a1* gene in the mouse kidneys and pericyte-like cells and induces profibrotic signaling in the pericytes. The binding of STAT3 on specific DNA sequences during fibrosis progression needs further investigation to understand the dynamics of the whole genome occupancy. Thus, in this study we have identified a crucial role of STAT3 phosphorylation in increasing profibrotic signaling in the Foxd1 lineage. These findings provide potential therapeutic interventions of pericytes using STAT3 as a therapeutic target (Graphical Abstract).

Limitations of the study

The nuclear intensity as shown by DAPI changes due to tissue damage in fibrotic kidneys. In general, we found significant increased background in paraffin embedded kidneys as compared to OCT embedded kidneys. We found it technically challenging for co-immunostaining for NG2 antibodies which only works on OCT embedded kidney sections. We used mouse pericytes cell line for our study but availability of human pericyte cell line may provide more relevance to the human fibrotic disease.

STAR METHODS

Resource availability

Lead contact—Further information and requests for resources and reagents should be directed to and will be fulfilled by the Lead Contact, Amrendra K. Ajay (akajay@bwh.harvard.edu)

Materials availability

All unique/stable reagents generated in this study are available from the Lead Contact with a completed Materials Transfer Agreement.

Experimental model and subject details

Cell line—10T1/2 a pericyte-like cells was purchased from ATCC (Manassas, VA) and maintained in BME medium with 10% FBS and 2 mg/ml sodium pyruvate. Cells were grown in a 37°C incubator with 5% CO_2 and 37% relative humidity.

Human subjects—Human kidney biopsy sections were obtained through Brigham and Women's Hospital's pathology service core, and they were classified as patients without evidence of ATN as healthy (n=10), patients with evidence of Acute Tubular Necrosis (ATN) as AKI (n=5) and patients with Diabetic Nephropathy (DN) as CKD (n=10). Samples were collected by patient consent and include both male and female gender aged between 42–68. The Institutional Review Board approved the protocol for extracting paraffin-embedded, formalin-fixed sections from patients with and without ATN and DN.

Mice—Male C57BL/6J mice (age 8–10 weeks) were purchased from the Jackson Laboratory (Bar Harbor, ME). *Stat3*^{flox} (*Stat3*^{fl}) mice were a kind gift from Dr. Kevin Haigis (Dana Farber Cancer Institute, Boston, MA) and *Foxd1*^{GC} mice were a kind gift from Dr. Benjamin D. Humphreys (Washington University in St. Louis, MO). *Stat3* homozygous and *Foxd1* heterozygous mice were bred to generate *Foxd1*^{GC} *Stat3*$^{fl/fl}$ (*Stat3* KO) mice in *Foxd1*-positive cell population. *Stat3* homozygous mice without *Foxd1 cre* allele named as *Stat3*$^{fl/fl}$ (control) mice were used as littermate controls. Mice were treated with single dose of either 250 mg/kg body weight of folic acid or 5 mg/kg body weight of aristolochic acid intraperitonially and blood was collected at acute and chronic phases of injuries. Mice were injected with 50 mg/kg body weight of BrdU, 3 hrs prior to sacrifice as previously described (Ajay et al., 2012). Mice were sacrificed and kidneys were harvested at day 7 and 14 post-treatments. All the experiments were conducted with the approval and guidelines of

IACUC and Center for Comparative Medicine of Brigham and Women's Hospital and were housed in a facility equipped with a 12-hour light/dark cycle.

Method details

Estimation of blood urea nitrogen and serum creatinine—BUN and sCr were measured at the National Institutes of Health-sponsored George O'Brian Centre for Acute Kidney Injury Research Core at University of California, San Diego, San Diego, CA and University of Alabama, Birmingham, AL, respectively. BUN estimation: The Bio Assay Systems Quantitative Colorimetric Urea Determination kit (DIUR-100) was used for the estimation for BUN. It is based on modified Jung method (Jung et al., 1975) that utilizes a chromogenic reagent. This chromogen forms a colored complex specifically with urea and the intensity of the color, measured at 520nm, is directly proportional to the urea concentration in the sample. Conversions: BUN (mg/dL) = [Urea] / 2.14. 1mg/dL urea equals 167μM, 0.001% or 10ppm.

sCr estimation: For measurement of sCr, LC-MS/MS (6460C Triple Quad Mass Spectrometer, Agilent Technologies, Wilmington, DE) was used. 5 to 50μl of sample were deproteinated and diluted with heavy isotope-labeled internal standard (ISTD) in a single step by adding ISTD in 80% acetonitrile. Two microliters of diluted sample were subjected to isocratic, HILIC HPLC (Infinity 1260 LC, Agilent Technologies, Wilmington, DE) with 10 mM ammonium acetate in 65% acetonitrile at 0.15ml/min. Creatinine and d_3-creatinine (ISTD) were detected by electrospray ionization tandem mass spectrometry MRM transitions 114 > 44 and 117 > 47, respectively. Quantitation was achieved by comparing results to a synthetic standard calibration curve (0, 0.2, 1, 5, 100μg/ml for serum) (Young et al., 2007).

Fibrosis characterization

Histology: Periodic Acid-Schiff (PAS) stain and Mason's Trichrome staining (MTS) was performed at Harvard rodent pathology core. Images were captured by a Nikon DS-Qi1Mc camera attached to a Nikon Eclipse 90i fluorescence microscope using an 40X or 60X objective using Nikon NIS elements AR version 3.2 software.

Interstitial Fibrosis and Tubular Atrophy (IFTA) scoring: Scores for interstitial fibrosis and tubular atrophy was performed by microscopic observation of the kidney sections under 200X magnification. The area of interstitial fibrosis was evaluated by Masson's Trichrome Staining and higher scores were assigned for higher staining areas. Tubular atrophy was evaluated by PAS staining and scores were assigned. The scores ranged from 0 to 4, where 0 is no IFTA and 4 is severe IFTA, in comparison to mice without any injury. IFTA scores were performed by two pathologist and average values of the scores were plotted.

Chemical and antibodies

Chemicals: IL-6 was purchased from R&D Systems (Minneapolis, MN) and resuspended as per manufacturer's instructions. Stattic was purchased from Millipore Sigma (Burlington, MA) and dissolved in DMSO. Phalloidin (cat. no. R415) and Cell Tracker Green Dye

(cat. no. C2925) was purchased from Thermo Fisher Scientific (Waltham, MA). LTL was purchased from Vector laboratories (cat. no. NC0127927).

Antibodies: Anti-pSTAT3 Tyrosine 705 (cat. no. 9145) and anti-STAT3 (cat. no. 9139), anti-Ki67 (cat. no. 9449), anti-F4/80 (cat. no. 30325), pH2AX (cat. no. 9718), pSMAD2 (cat. no. 18338) were purchased from Cell Signaling Technology (Danvers, MA). Anti-Fibronectin (cat. no. ab2413), anti-Collagen1 (cat. no. ab34710) and anti-Na^+ K^+ ATPase (cat. no. ab76020) were purchased from Abcam (Cambridge, MA). Anti-α-SMA (cat. no. A5228) and anti-GAPDH (cat. no. SAB2108668–100UL) were purchased from Thermo Fisher Scientific. Horse Radish Peroxidase (HRP) conjugated anti-rabbit (cat. no. 7074) and anti-mouse (cat. no. 7076) antibodies were purchased from Cell Signaling Technology. Anti-Rabbit, anti-rat, or anti-mouse Alexa488, Alexa 594 and Alexa 647 conjugated antibodies were purchased from Thermo Fisher Scientific. For co-immunostaining using the same species antibodies, primary antibodies were conjugated using Lightning-Link® Rapid Alexa Fluor 488 Antibody Labeling Kit (Novus Biologicals, Centennial, CO 80112).

CRISPR-mediated gain and loss-of-function

CRISPR-mediated *Stat3* KO: sgRNAs were designed using Broad Institute/MIT CRISPR design tool (http://crispr.mit.edu) for the genomic location around transcription start site in exon 1. sgRNAs were cloned into pSpCas9(BB)-2A-GFP plasmid (Addgene, Watertown, MA). Genomic DNA was extracted using the PureLink® Genomic DNA Mini Kit (cat. no. K182002, Thermo Fisher Scientific). PCR was performed using *Stat3* KO primers described in Supplementary Table 1. The deletion was confirmed by DNA sequencing followed by western blotting of STAT3 (Figures S5A–S5C).

Cells were transfected with the designed plasmid and incubated for 48 hours with plasmids. Single cells positive for GFP were then sorted into a 96-well plate and were grown for 14 days with changing media every 4–5 days. Cells were then stained with pSTAT3 antibodies to confirm the expression levels of phosphorylated STAT3. Positive clones were selected for further studies.

CRISPR-mediated Synergistic Activation Mediators (SAM): For CRISPR-mediated SAM, sgRNAs were designed for promoter region of *Stat3* (https://epd.epfl.ch//index.php) as discussed in the previous section and 4 residues were removed from 5’ end to make it a 16 nucleotide sgRNA. The 16-base pair sgRNA loses its capability to break the genomic DNA but retains the binding ability to specific DNA sequence (Dahlman et al., 2015). Two sgRNAs from proximal, central, and distal promoter regions were selected and were cloned into the lenti-CRISPRV2 plasmid (Addgene). Lentivirus was produced in HEK293 cells by transfecting lenti-CRISPRV2, VSV-G, REV, and GAG plasmids. The supernatant after incubation for 48 hours was collected and centrifuged to get the clear supernatant containing viral particles.

Pericyte-like cells, 10T1/2, were transduced with the lentiviral particles. SAM activation plasmid containing MS2-p65-HSF1-VP64 was co-transfected in the cells along with the lentiviral particles. *Stat3* gene expression was confirmed by PCR amplification using

TaqMan probes described in Supplementary Table 1 and immunostaining with STAT3 Tyrosine 705 was performed at 72-hours post-transductions.

CRISPR-mediated mutation to generate STAT3-C: sgRNAs were designed by selecting the genomic location of Alanine662 and Asparagine664. sgRNAs were cloned into the pSpCas9(BB)-2A-GFP plasmid. Ultramers containing these two mutations to Cysteines were synthesized and co-transfected with the plasmid. GFP-positive cells were sorted and were grown as single cell clones as described above. Immunostaining for pSTAT3 was performed to identify the cells with increased pSTAT3. List of sgRNAs and ultramers is shown in Supplementary Table 1.

Isolation of kidney pericytes and kidney resident macrophage using FACS— Control and *Stat3* KO mice were sacrificed at day 14 post-AA treatment and perfused with ice-cold PBS. Immediately, the kidneys were harvested and digested with Iscove's Modified Dulbecco's Medium (IMDM) (Gibco) containing Collagenase D (2.5 mg/ml, Roche Diagnostics) and DNase I (1 mg/ml, Sigma-Aldrich) at 37°C for 45 min. Digested tissue was passed through a 70μm cell strainer and centrifuged at 1600 rpm for 5 min at 4°C. Pellets were resuspend in 37% Percoll (GE Healthcare) and overlaid on top of 70% Percoll and centrifuged at 2000 rpm for 25 min at RT with no brake for gradient centrifugation. Mononuclear cells at the interphase were collected and washed twice with cold Hank's Buffered Saline Solution (HBSS, Gibco). Samples were split in two, one for macrophage sorting and the other for pericyte sorting. Cells at the bottom of the tubes were also collected, washed twice with cold HBSS and included in the pericyte sorting. For pericyte sorting, cells were stained with 7-AAD, anti-CD45-PerCP, anti-CD3-PerCP, anti-NK1.1-PerCP, anti-CD19-PerCP, anti-CD31-PE, anti-CD140b-APC, and anti-NG2-Alexa Fluor 488. For macrophage sorting, cells were stained with 7-AAD, anti-CD45-PE-Cy7, anti-MHC II-APC-Cy7, anti-CD11b-PE, and anti-F4/80-APC. Cells were then sorted using FACSAria IIu Cell Sorter (Becton Dickinson) using 100μm nozzle. Collected cells were lysed with RLT buffer containing 1% β-mercaptoethanol.

Scratch assay—10T1/2 cells were plated in a 6-well plate at a confluency of 80% and the next day a scratch was created with a 200μl microtip. Cells were washed three times with PBS and treated with IL-6 and stattic for 12 hours. Cells were fixed and images were taken using Nikon Eclipse 90i microscope using 10X objective.

Transwell migration assay—10T1/2 cells were plated in 6-well plates and serum starved for 16 hours. Ten thousand cells were then plated onto the upper well of 8μm pore transwell inserts (BD Bioscience). The lower chamber contained either control medium, medium with IL-6 (100 ng/ml), or medium with IL-6 (100 ng/ml) and stattic (2.5 μM). Cells were incubated for an additional 12 hours. Using a cotton swab the cells from the upper wells were removed and were fixed with 4% paraformaldehyde. Cells were then stained with CellMask Green (1:10,000 dilution, Thermo Fisher Scientific) and were imaged using Nikon Eclipse 90i microscope using 10X objective after removing the cells from the insert and fixing them on a glass slide.

Western blotting—Western blotting was performed as previously described (Ajay et al., 2014b). Briefly, kidney tissue or cells were lysed using RIPA buffer containing protease and phosphatase inhibitors. Tissue was homogenized using homogenizer. Cell lysates were cleared using centrifugation and equal protein was loaded onto the gel. Protein was transferred onto the PVDF membrane and probed with specific antibodies. GAPDH or β-Actin were used as a loading control. Blots were developed using Luminata Forte HRP reagent using a Bio-Rad (Hercules, CA) or Syngene (Fredrick, MD) imaging systems. Quantification of blots was performed using Image lab for Bio-Rad or GeneSys for Syngene software and the data was normalized to the loading controls to calculate the fold change.

RNA isolation, cDNA synthesis, and quantitative Real-Time PCR—Total RNA was isolated from cell pellets using the RNeasy Micro or Mini Kit (Qiagen, Germantown, MD) and first-strand cDNA synthesis was performed for each RNA sample from 0.5 to 1μg of total RNA using TaqMan reverse transcription reagents.

TaqMan RT-PCR: RNA from kidney tissue or cells was isolated using miRNeasy Mini Kit (Qiagen, Germantown, MD) as per manufacturer's instruction. Five hundred nanograms of total RNA was converted into cDNA using High-Capacity cDNA Reverse Transcription Kits (Applied Biosystems, Thermo Fisher Scientific) according to manufacturer's protocol. Two microliters of five times diluted cDNA were used for PCR using TaqMan™ Universal PCR Master Mix with FAM-labeled gene specific probes (Thermo Fisher Scientific) in duplicate on a QuantStudio 7 thermal cycler (Thermo Fisher Scientific). Fold change was calculated by delta Ct methods with *Gapdh* as the reference gene and presented as fold change with respect to experimental controls.

RT-PCR: For genotyping, DNA was extracted from mouse tail samples using Kappa Genotyping Kit in duplicate (Roche, Basel, Switzerland) as per manufacturer's instructions and RT-PCR was performed using specific primers described in Supplementary Table 1. PCR products were resolved onto agarose gel and imaged using Bio-Rad gel imaging system ChemiDoc MP.

Immunofluorescence staining

Immunofluorescence staining: Immunofluorescence on OCT of paraffin tissue sections or cells were performed as previously described (Ajay et al., 2014b; Ajay et al., 2012; Craciun et al., 2014). Briefly, formalin-fixed paraffin-embedded tissue sections were deparaffinized using xylene and followed by antigen retrieval using citrate buffer. For the OCT block from PFA-fixed tissue sections, PBS was added to the slides and antigen retrieval was performed using proteinase K treatment. For staining the cells, 4% PFA was used for fixation. Samples were permeabilized using 1% Triton X-100 for 15 min. Two percent normal sheep serum containing 5% BSA was used for blocking for 1 hour. Primary antibodies were incubated overnight at 4°C in five times diluted blocking buffer containing 0.1% Tween 20. After three washes of PBST (0.1% Tween 20), fluorescence-labeled secondary antibodies (Thermo Fisher Scientific) were added and incubated for 1 hour at room temperature. Slides were washed and mounted with medium containing DAPI (Vector laboratories). Three-to-five images were captured using 60X objective either on a Nikon Confocal Imaging system

(Nikon C1 Eclipse, Nikon, Melville, NY) or Axio Imager A2m widefield microscope (Carl Zeiss, White Plains, NY).

DNA sequence analysis—DNA sequencing data was viewed using SnapGene Viewer to obtain the chromatograms. Sequences were aligned using pairwise alignment tool using Needle (https://www.ebi.ac.uk/Tools/psa/emboss_needle).

Periodic Acid Schiff staining—PAS staining was performed at Rodent Histology Core, Harvard Medical School, Boston, MA. Briefly, formalin-fixed paraffin-embedded tissue sections, and may be used for frozen sections as well. Tissue sections were deparaffinized and hydrated to water in series of Xylenes gradual increased in hydrated ethanol. Oxidized in 0.5% Periodic Acid (Cat. No. 379891, Millipore Sigma) solution for 5 minutes. Slides were rinsed in 3 changes of distilled water and placed in Schiff's reagent (Cat no. 50–301-27, Fisher Scientific) for 15 minutes. Sectionwere were washed in tap water for 5 minutes Counterstaining in Mayer's hematoxylin (Cat. no. NC9220898, Fisher Scientific) for 1 minute was performed and washed in tap water for 5 min. Sections were dehydrated in gradual increase in ethanol and mounted using xylene based mounting media.

Low magnification kidney section imaging—Images were captured with an Incucyte Zoom widefield microscope (Essen Biosciences) using the software version is 2016B and were stitched together to obtain the combined image for the whole section.

BrdU incorporation assay—BrdU incorporation assay was performed as per manufacturer's protocol (Abcam). Briefly, two thousand cells were plated in a 96-well plate and 2 hours before endpoints, BrdU was added. Cells were fixed and anti-BrdU antibody was added and incubated at room temperature for 30 minutes. After washing, anti-mouse peroxidase IgG was added, and washing was repeated. TMB substrate was added and incubated in dark for 30 minutes at room temperature. The reaction was stopped by stop solution and the plate was read at 450nm. Control cells were referenced as 100% proliferation to plot the graphs.

Cell detachment assay—Cells were plated on chambered slides and incubated for 1 hour. Cells were then rotated on shaker for 15 minutes and washed thrice with PBS. Cells were fixed with 4% PFA and stained with phalloidin. Cells were then mounted with mounting medium containing DAPI. Images were captured using a Nikon confocal imaging system at 60X magnification. The number of cells present were counted, and graph were plotted.

Cell spreading assay—Cells were plated on chambered slides and incubated for 3 hours. Cells were fixed with 4% PFA and stained with phalloidin. Cells were then mounted with mounting medium containing DAPI. Images were captured using a Nikon confocal imaging system at 60X magnification. The area of cells was calculated using ImageJ software and graphs were plotted with respect to control cells.

In silico promoter analysis and ChIP sequencing analysis

***In silico* STAT3 binding prediction:** Promoter regions of *Collagen1a1* and *Fibronectin1* gene were extracted from (https://epd.epfl.ch//index.php) and a search was performed for STAT3 binding sites using (http://jaspar.genereg.net).

ChIP sequencing analysis: ChIP data was analyzed from previously performed STAT3 ChIP sequencing in normal mouse kidneys for promoter binding of *Collagen1a1* and *Fibronectin1* genes (Source data: GSM3176738, GSM3176739). Peaks on the log scale were shown as DNA binding sites for STAT3.

Chromatin Immunoprecipitation (ChIP) assay—ChIP assay was performed as previously described (Ajay et al., 2014b). Briefly, 3mm diameter of snap frozen kidney tissue or cells were treated with 1% formaldehyde/protease inhibitor DNA to crosslink proteins. Sonication was performed to get DNA fragments ranging from 200 to 1000 bp. Fifteen hundred μg protein was immunoprecipitated with 10μg STAT3, normal rabbit IgG (negative control), or RNA polymerase (positive control) antibodies. Fifteen micrograms (1%) protein from each sample was frozen in 80°C as input. Protein G was used to pull down bound immune complex and DNA was isolated. Five-microliter samples were used for real time PCR using promoter-specific primers of *Collagen1a1* gene promoter (Supplementary Table 1).

Luciferase assay—Cells were plated in a 12-well plate and were co-transfected with Firefly *STAT3* luciferase and Renilla *Gapdh* luciferase (gift from Dr. Matthias Brock, Center of Experimental Rheumatology, University Hospital Zurich, Zurich, Switzerland) plasmids. After 24 hours, cells were treated with IL-6 and stattic. Cells were harvested at 72 hours post-transfection and lysed using passive lysis buffer using Dual-Luciferase Reporter assay purchased from Promega (Madison, WI). Luciferase assay was performed as previously described (Ajay et al., 2014b). Ratio of Firefly and Renilla luciferase readings were plotted with respect to control cells.

Supplementary Table: Related to Figures 2, 3, 5, S2, S3 and S5—List of primers for CRISPR mediated gene editing, TaqMan based primers and genotyping.

Quantitation and statistical analysis

Quantitation of immunostaining: The intensity of the respective channels was calculated after setting up a threshold for all the images. The intensity was normalized to total number of cells by counting the DAPI-positive cells. For double-positive cells with one nuclear and one cytoplasmic stain, the counting was performed by manual tagging of the positive cells and percentages were calculated as compared to control samples using Image J software. The fold change was plotted with respected to the control samples. For counting tubular and interstitial cells, the total number of positive cells were counted: the tubular mask was generated either by Na^+ K^+ ATPase (for pSTAT3) or tubular background (for pH2AX and Ki67) and tubular cells were counted manually. For calculating the interstitial cells, tubular positive cells were subtracted from total positive cells.

Statistical analyses: Statistical analyses were performed using a two-tailed unpaired T-Test to compare two groups. A *p*-value of less than or equal to 0.05 was considered statistically significant. Data are presented as the mean ± SD. Please see individual figure captions for more details. GraphPad Prism 9.0 (GraphPad Software, Inc., La Jolla, CA) was used for all statistical analyses.

Data and code availability

- No high throughput datasets were generated for this publication.
- No new custom code was generated for this publication.

Supplementary Material

Refer to Web version on PubMed Central for supplementary material.

ACKNOWLEDGEMENTS

This research was supported by a center grant to LH. AA is supported by a Career Development Grant from the American Heart Association (19CDA34780005). LZ is supported by the National Science Foundation, China. The research in Gopal lab is supported by the grants from the NIH (R01 AI435801 and R01 AI151953). VS is supported by an R01 from the NCI.

REFERENCES

Ajay AK, Kim TM, Ramirez-Gonzalez V, Park PJ, Frank DA, and Vaidya VS (2014a). A bioinformatics approach identifies signal transducer and activator of transcription-3 and checkpoint kinase 1 as upstream regulators of kidney injury molecule-1 after kidney injury. Journal of the American Society of Nephrology : JASN 25, 105–118. [PubMed: 24158981]

Ajay AK, Kim TM, Ramirez-Gonzalez V, Park PJ, Frank DA, and Vaidya VS (2014b). A bioinformatics approach identifies signal transducer and activator of transcription-3 and checkpoint kinase 1 as upstream regulators of kidney injury molecule-1 after kidney injury. J Am Soc Nephrol 25, 105–118. [PubMed: 24158981]

Ajay AK, Saikumar J, Bijol V, and Vaidya VS (2012). Heterozygosity for fibrinogen results in efficient resolution of kidney ischemia reperfusion injury. PLoS One 7, e45628.

Anorga S, Overstreet JM, Falke LL, Tang J, Goldschmeding RG, Higgins PJ, and Samarakoon R. (2018). Deregulation of Hippo-TAZ pathway during renal injury confers a fibrotic maladaptive phenotype. FASEB journal : official publication of the Federation of American Societies for Experimental Biology 32, 2644–2657. [PubMed: 29298862]

Artaza JN, Singh R, Ferrini MG, Braga M, Tsao J, and Gonzalez-Cadavid NF (2008). Myostatin promotes a fibrotic phenotypic switch in multipotent C3H 10T1/2 cells without affecting their differentiation into myofibroblasts. J Endocrinol 196, 235–249. [PubMed: 18252947]

Asada N, Takase M, Nakamura J, Oguchi A, Asada M, Suzuki N, Yamamura K, Nagoshi N, Shibata S, Rao TN, et al. (2011). Dysfunction of fibroblasts of extrarenal origin underlies renal fibrosis and renal anemia in mice. J Clin Invest 121, 3981–3990. [PubMed: 21911936]

Bienaime F, Muorah M, Yammine L, Burtin M, Nguyen C, Baron W, Garbay S, Viau A, Broueilh M, Blanc T, et al. (2016). Stat3 Controls Tubulointerstitial Communication during CKD. J Am Soc Nephrol 27, 3690–3705. [PubMed: 27153926]

Campanholle G, Ligresti G, Gharib SA, and Duffield JS (2013). Cellular mechanisms of tissue fibrosis. 3. Novel mechanisms of kidney fibrosis. Am J Physiol Cell Physiol 304, C591–603. [PubMed: 23325411]

Centers for Disease, C., and Prevention (2007). Prevalence of chronic kidney disease and associated risk factors--United States, 1999–2004. MMWR Morb Mortal Wkly Rep 56, 161–165. [PubMed: 17332726]

Chakraborty D, Sumova B, Mallano T, Chen CW, Distler A, Bergmann C, Ludolph I, Horch RE, Gelse K, Ramming A, et al. (2017). Activation of STAT3 integrates common profibrotic pathways to promote fibroblast activation and tissue fibrosis. Nature communications 8, 1130.

Chen J, Chen JK, Nagai K, Plieth D, Tan M, Lee TC, Threadgill DW, Neilson EG, and Harris RC (2012). EGFR signaling promotes TGFbeta-dependent renal fibrosis. Journal of the American Society of Nephrology : JASN 23, 215–224. [PubMed: 22095949]

Chen J, Wang X, He Q, Bulus N, Fogo AB, Zhang MZ, and Harris RC (2020a). YAP Activation in Renal Proximal Tubule Cells Drives Diabetic Renal Interstitial Fibrogenesis. Diabetes 69, 2446–2457. [PubMed: 32843569]

Chen J, You H, Li Y, Xu Y, He Q, and Harris RC (2018). EGF Receptor-Dependent YAP Activation Is Important for Renal Recovery from AKI. J Am Soc Nephrol 29, 2372–2385. [PubMed: 30072422]

Chen TK, Estrella MM, Appel LJ, Coresh J, Luo S, Obeid W, Parikh CR, and Grams ME (2020b). Serum levels of interleukin (IL)-6, IL-8 and IL-10 and risks of end-stage kidney disease and mortality. Nephrol Dial Transplant.

Chung S, Overstreet JM, Li Y, Wang Y, Niu A, Wang S, Fan X, Sasaki K, Jin GN, Khodo SN, et al. (2018). TGF-beta promotes fibrosis after severe acute kidney injury by enhancing renal macrophage infiltration. JCI Insight 3.

Collier JB, and Schnellmann RG (2017). Extracellular Signal-Regulated Kinase 1/2 Regulates Mouse Kidney Injury Molecule-1 Expression Physiologically and Following Ischemic and Septic Renal Injury. J Pharmacol Exp Ther 363, 419–427. [PubMed: 29074644]

Coresh J, Astor BC, Greene T, Eknoyan G, and Levey AS (2003). Prevalence of chronic kidney disease and decreased kidney function in the adult US population: Third National Health and Nutrition Examination Survey. Am J Kidney Dis 41, 1–12. [PubMed: 12500213]

Coresh J, Byrd-Holt D, Astor BC, Briggs JP, Eggers PW, Lacher DA, and Hostetter TH (2005). Chronic kidney disease awareness, prevalence, and trends among U.S. adults, 1999 to 2000. J Am Soc Nephrol 16, 180–188. [PubMed: 15563563]

Coresh J, Selvin E, Stevens LA, Manzi J, Kusek JW, Eggers P, Van Lente F, and Levey AS (2007). Prevalence of chronic kidney disease in the United States. JAMA 298, 2038–2047. [PubMed: 17986697]

Craciun FL, Ajay AK, Hoffmann D, Saikumar J, Fabian SL, Bijol V, Humphreys BD, and Vaidya VS (2014). Pharmacological and genetic depletion of fibrinogen protects from kidney fibrosis. Am J Physiol Renal Physiol 307, F471–484. [PubMed: 25007874]

Dahlman JE, Abudayyeh OO, Joung J, Gootenberg JS, Zhang F, and Konermann S. (2015). Orthogonal gene knockout and activation with a catalytically active Cas9 nuclease. Nat Biotechnol 33, 1159–1161. [PubMed: 26436575]

Dalla Vestra M, Mussap M, Gallina P, Bruseghin M, Cernigoi AM, Saller A, Plebani M, and Fioretto P. (2005). Acute-phase markers of inflammation and glomerular structure in patients with type 2 diabetes. Journal of the American Society of Nephrology : JASN 16 *Suppl* 1, S78–82. [PubMed: 15938041]

Ding J, Su S, You T, Xia T, Lin X, Chen Z, and Zhang L. (2020). Serum interleukin-6 level is correlated with the disease activity of systemic lupus erythematosus: a meta-analysis. Clinics (Sao Paulo) 75, e1801. [PubMed: 33084768]

DiRocco DP, Kobayashi A, Taketo MM, McMahon AP, and Humphreys BD (2013). Wnt4/beta-catenin signaling in medullary kidney myofibroblasts. Journal of the American Society of Nephrology : JASN 24, 1399–1412. [PubMed: 23766539]

Do DV, Ueda J, Messerschmidt DM, Lorthongpanich C, Zhou Y, Feng B, Guo G, Lin PJ, Hossain MZ, Zhang W, et al. (2013). A genetic and developmental pathway from STAT3 to the OCT4-NANOG circuit is essential for maintenance of ICM lineages in vivo. Genes Dev 27, 1378–1390. [PubMed: 23788624]

Do NN, Willenborg S, Eckes B, Jungst C, Sengle G, Zaucke F, and Eming SA (2018). Myeloid Cell-Restricted STAT3 Signaling Controls a Cell-Autonomous Antifibrotic Repair Program. J Immunol 201, 663–674. [PubMed: 29898959]

Dube S, Matam T, Yen J, Mang HE, Dagher PC, Hato T, and Sutton TA (2017). Endothelial STAT3 Modulates Protective Mechanisms in a Mouse Ischemia-Reperfusion Model of Acute Kidney Injury. J Immunol Res 2017, 4609502.

Duffield JS, and Humphreys BD (2011). Origin of new cells in the adult kidney: results from genetic labeling techniques. Kidney Int 79, 494–501. [PubMed: 20861816]

E O.h., and Humphreys BD (2017). Fibrotic Changes Mediating Acute Kidney Injury to Chronic Kidney Disease Transition. Nephron 137, 264–267. [PubMed: 28595180]

El Agha E, Kramann R, Schneider RK, Li X, Seeger W, Humphreys BD, and Bellusci S. (2017). Mesenchymal Stem Cells in Fibrotic Disease. Cell stem cell 21, 166–177. [PubMed: 28777943]

Fabian SL, Penchev RR, St-Jacques B, Rao AN, Sipila P, West KA, McMahon AP, and Humphreys BD (2012). Hedgehog-Gli pathway activation during kidney fibrosis. Am J Pathol 180, 1441–1453. [PubMed: 22342522]

Gao H, Bryzgalova G, Hedman E, Khan A, Efendic S, Gustafsson JA, and Dahlman-Wright K. (2006). Long-term administration of estradiol decreases expression of hepatic lipogenic genes and improves insulin sensitivity in ob/ob mice: a possible mechanism is through direct regulation of signal transducer and activator of transcription 3. Mol Endocrinol 20, 1287–1299. [PubMed: 16627594]

Gewin L, Bulus N, Mernaugh G, Moeckel G, Harris RC, Moses HL, Pozzi A, and Zent R. (2010). TGF-beta receptor deletion in the renal collecting system exacerbates fibrosis. Journal of the American Society of Nephrology : JASN 21, 1334–1343. [PubMed: 20576806]

Gewin LS (2018). Renal Tubule Repair: Is Wnt/beta-Catenin a Friend or Foe? Genes (Basel) 9.

Gu L, Dai Y, Xu J, Mallipattu S, Kaufman L, Klotman PE, He JC, and Chuang PY (2013). Deletion of podocyte STAT3 mitigates the entire spectrum of HIV-1-associated nephropathy. AIDS 27, 1091–1098. [PubMed: 23343908]

Hao S, He W, Li Y, Ding H, Hou Y, Nie J, Hou FF, Kahn M, and Liu Y. (2011). Targeted inhibition of beta-catenin/CBP signaling ameliorates renal interstitial fibrosis. Journal of the American Society of Nephrology : JASN 22, 1642–1653. [PubMed: 21816937]

Happe H, Leonhard WN, van der Wal A, van de Water B, Lantinga-van Leeuwen IS, Breuning MH, de Heer E, and Peters DJ (2009). Toxic tubular injury in kidneys from Pkd1-deletion mice accelerates cystogenesis accompanied by dysregulated planar cell polarity and canonical Wnt signaling pathways. Hum Mol Genet 18, 2532–2542. [PubMed: 19401297]

He W, Dai C, Li Y, Zeng G, Monga SP, and Liu Y. (2009). Wnt/beta-catenin signaling promotes renal interstitial fibrosis. Journal of the American Society of Nephrology : JASN 20, 765–776. [PubMed: 19297557]

Henderson NC, Arnold TD, Katamura Y, Giacomini MM, Rodriguez JD, McCarty JH, Pellicoro A, Raschperger E, Betsholtz C, Ruminski PG, et al. (2013). Targeting of alphav integrin identifies a core molecular pathway that regulates fibrosis in several organs. Nat Med 19, 1617–1624. [PubMed: 24216753]

Humphreys BD, Lin SL, Kobayashi A, Hudson TE, Nowlin BT, Bonventre JV, Valerius MT, McMahon AP, and Duffield JS (2010). Fate tracing reveals the pericyte and not epithelial origin of myofibroblasts in kidney fibrosis. Am J Pathol 176, 85–97. [PubMed: 20008127]

Ichiba M, Nakajima K, Yamanaka Y, Kiuchi N, and Hirano T. (1998). Autoregulation of the Stat3 gene through cooperation with a cAMP-responsive element-binding protein. J Biol Chem 273, 6132–6138. [PubMed: 9497331]

Jacoby JJ, Kalinowski A, Liu MG, Zhang SS, Gao Q, Chai GX, Ji L, Iwamoto Y, Li E, Schneider M, et al. (2003). Cardiomyocyte-restricted knockout of STAT3 results in higher sensitivity to inflammation, cardiac fibrosis, and heart failure with advanced age. Proc Natl Acad Sci U S A 100, 12929–12934. [PubMed: 14566054]

Jung D, Biggs H, Erikson J, and Ledyard PU (1975). New Colorimetric reaction for end-point, continuous-flow, and kinetic measurement of urea. Clin Chem 21, 1136–1140. [PubMed: 1137920]

Kasembeli MM, Bharadwaj U, Robinson P, and Tweardy DJ (2018). Contribution of STAT3 to Inflammatory and Fibrotic Diseases and Prospects for its Targeting for Treatment. Int J Mol Sci 19.

Kida Y, and Duffield JS (2011). Pivotal role of pericytes in kidney fibrosis. Clin Exp Pharmacol Physiol 38, 467–473. [PubMed: 21517936]

Kobayashi A, Mugford JW, Krautzberger AM, Naiman N, Liao J, and McMahon AP (2014). Identification of a multipotent self-renewing stromal progenitor population during mammalian kidney organogenesis. Stem Cell Reports 3, 650–662. [PubMed: 25358792]

Kramann R, DiRocco DP, and Humphreys BD (2013). Understanding the origin, activation and regulation of matrix-producing myofibroblasts for treatment of fibrotic disease. J Pathol 231, 273–289. [PubMed: 24006178]

Kramann R, Fleig SV, Schneider RK, Fabian SL, DiRocco DP, Maarouf O, Wongboonsin J, Ikeda Y, Heckl D, Chang SL, et al. (2015a). Pharmacological GLI2 inhibition prevents myofibroblast cell-cycle progression and reduces kidney fibrosis. J Clin Invest 125, 2935–2951. [PubMed: 26193634]

Kramann R, and Humphreys BD (2014). Kidney pericytes: roles in regeneration and fibrosis. Semin Nephrol 34, 374–383. [PubMed: 25217266]

Kramann R, Schneider RK, DiRocco DP, Machado F, Fleig S, Bondzie PA, Henderson JM, Ebert BL, and Humphreys BD (2015b). Perivascular Gli1+ progenitors are key contributors to injury-induced organ fibrosis. Cell stem cell 16, 51–66. [PubMed: 25465115]

LeBleu VS, Taduri G, O'Connell J, Teng Y, Cooke VG, Woda C, Sugimoto H, and Kalluri R. (2013). Origin and function of myofibroblasts in kidney fibrosis. Nat Med 19, 1047–1053. [PubMed: 23817022]

Lee HK, Willi M, Shin HY, Liu C, and Hennighausen L. (2018). Progressing super-enhancer landscape during mammary differentiation controls tissue-specific gene regulation. Nucleic Acids Res 46, 10796–10809. [PubMed: 30285185]

Leu CM, Wong FH, Chang C, Huang SF, and Hu CP (2003). Interleukin-6 acts as an antiapoptotic factor in human esophageal carcinoma cells through the activation of both STAT3 and mitogen-activated protein kinase pathways. Oncogene 22, 7809–7818. [PubMed: 14586407]

Lin J, Patel SR, Cheng X, Cho EA, Levitan I, Ullenbruch M, Phan SH, Park JM, and Dressler GR (2005). Kielin/chordin-like protein, a novel enhancer of BMP signaling, attenuates renal fibrotic disease. Nat Med 11, 387–393. [PubMed: 15793581]

Lin SL, Chang FC, Schrimpf C, Chen YT, Wu CF, Wu VC, Chiang WC, Kuhnert F, Kuo CJ, Chen YM, et al. (2011). Targeting endothelium-pericyte cross talk by inhibiting VEGF receptor signaling attenuates kidney microvascular rarefaction and fibrosis. Am J Pathol 178, 911–923. [PubMed: 21281822]

Lin SL, Kisseleva T, Brenner DA, and Duffield JS (2008). Pericytes and perivascular fibroblasts are the primary source of collagen-producing cells in obstructive fibrosis of the kidney. Am J Pathol 173, 1617–1627. [PubMed: 19008372]

Liu N, He S, Tolbert E, Gong R, Bayliss G, and Zhuang S. (2012). Suramin alleviates glomerular injury and inflammation in the remnant kidney. PLoS One 7, e36194.

Maarouf OH, Aravamudhan A, Rangarajan D, Kusaba T, Zhang V, Welborn J, Gauvin D, Hou X, Kramann R, and Humphreys BD (2016). Paracrine Wnt1 Drives Interstitial Fibrosis without Inflammation by Tubulointerstitial Cross-Talk. Journal of the American Society of Nephrology : JASN 27, 781–790. [PubMed: 26204899]

Mack M, and Yanagita M. (2015). Origin of myofibroblasts and cellular events triggering fibrosis. Kidney Int 87, 297–307. [PubMed: 25162398]

Madan B, Patel MB, Zhang J, Bunte RM, Rudemiller NP, Griffiths R, Virshup DM, and Crowley SD (2016). Experimental inhibition of porcupine-mediated Wnt O-acylation attenuates kidney fibrosis. Kidney Int 89, 1062–1074. [PubMed: 27083283]

Magno AL, Herat LY, Carnagarin R, Schlaich MP, and Matthews VB (2019). Current Knowledge of IL-6 Cytokine Family Members in Acute and Chronic Kidney Disease. Biomedicines 7.

Narimatsu M, Maeda H, Itoh S, Atsumi T, Ohtani T, Nishida K, Itoh M, Kamimura D, Park SJ, Mizuno K, et al. (2001). Tissue-specific autoregulation of the stat3 gene and its role in interleukin-6-induced survival signals in T cells. Mol Cell Biol 21, 6615–6625. [PubMed: 11533249]

Navarro JF, Milena FJ, Mora C, Leon C, and Garcia J. (2006). Renal pro-inflammatory cytokine gene expression in diabetic nephropathy: effect of angiotensin-converting enzyme inhibition and pentoxifylline administration. Am J Nephrol 26, 562–570. [PubMed: 17167242]

Nechemia-Arbely Y, Barkan D, Pizov G, Shriki A, Rose-John S, Galun E, and Axelrod JH (2008). IL-6/IL-6R axis plays a critical role in acute kidney injury. Journal of the American Society of Nephrology : JASN 19, 1106–1115. [PubMed: 18337485]

Nlandu-Khodo S, Neelisetty S, Phillips M, Manolopoulou M, Bhave G, May L, Clark PE, Yang H, Fogo AB, Harris RC, et al. (2017). Blocking TGF-beta and beta-Catenin Epithelial Crosstalk Exacerbates CKD. Journal of the American Society of Nephrology : JASN 28, 3490–3503. [PubMed: 28701516]

Okamoto M, Lee C, and Oyasu R. (1997). Interleukin-6 as a paracrine and autocrine growth factor in human prostatic carcinoma cells in vitro. Cancer Res 57, 141–146. [PubMed: 8988055]

Pace J, Paladugu P, Das B, He JC, and Mallipattu SK (2019). Targeting STAT3 signaling in kidney disease. Am J Physiol Renal Physiol 316, F1151–F1161. [PubMed: 30943069]

Pang M, Ma L, Gong R, Tolbert E, Mao H, Ponnusamy M, Chin YE, Yan H, Dworkin LD, and Zhuang S. (2010). A novel STAT3 inhibitor, S3I-201, attenuates renal interstitial fibroblast activation and interstitial fibrosis in obstructive nephropathy. Kidney Int 78, 257–268. [PubMed: 20520592]

Patel S, Tang J, Overstreet JM, Anorga S, Lian F, Arnouk A, Goldschmeding R, Higgins PJ, and Samarakoon R. (2019). Rac-GTPase promotes fibrotic TGF-beta1 signaling and chronic kidney disease via EGFR, p53, and Hippo/YAP/TAZ pathways. FASEB J 33, 9797–9810. [PubMed: 31095421]

Piersma B, Bank RA, and Boersema M. (2015). Signaling in Fibrosis: TGF-beta, WNT, and YAP/TAZ Converge. Front Med (Lausanne) 2, 59. [PubMed: 26389119]

Quan TE, Cowper SE, and Bucala R. (2006). The role of circulating fibrocytes in fibrosis. Curr Rheumatol Rep 8, 145–150. [PubMed: 16569374]

Sato M, Muragaki Y, Saika S, Roberts AB, and Ooshima A. (2003). Targeted disruption of TGF-beta1/Smad3 signaling protects against renal tubulointerstitial fibrosis induced by unilateral ureteral obstruction. J Clin Invest 112, 1486–1494. [PubMed: 14617750]

Schindelin J, Arganda-Carreras I, Frise E, Kaynig V, Longair M, Pietzsch T, Preibisch S, Rueden C, Saalfeld S, Schmid B, et al. (2012). Fiji: an open-source platform for biological-image analysis. Nat Methods 9, 676–682. [PubMed: 22743772]

Schrimpf C, and Duffield JS (2011). Mechanisms of fibrosis: the role of the pericyte. Curr Opin Nephrol Hypertens 20, 297–305. [PubMed: 21422927]

Seo E, Kim WY, Hur J, Kim H, Nam SA, Choi A, Kim YM, Park SH, Chung C, Kim J, et al. (2016). The Hippo-Salvador signaling pathway regulates renal tubulointerstitial fibrosis. Sci Rep 6, 31931. [PubMed: 27550469]

Shain KH, Yarde DN, Meads MB, Huang M, Jove R, Hazlehurst LA, and Dalton WS (2009). Beta1 integrin adhesion enhances IL-6-mediated STAT3 signaling in myeloma cells: implications for microenvironment influence on tumor survival and proliferation. Cancer Res 69, 1009–1015. [PubMed: 19155309]

Surendran K, Schiavi S, and Hruska KA (2005). Wnt-dependent beta-catenin signaling is activated after unilateral ureteral obstruction, and recombinant secreted frizzled-related protein 4 alters the progression of renal fibrosis. Journal of the American Society of Nephrology : JASN 16, 2373–2384. [PubMed: 15944336]

Takakura A, Nelson EA, Haque N, Humphreys BD, Zandi-Nejad K, Frank DA, and Zhou J. (2011). Pyrimethamine inhibits adult polycystic kidney disease by modulating STAT signaling pathways. Hum Mol Genet 20, 4143–4154. [PubMed: 21821671]

Wang N, Deng Y, Liu A, Shen N, Wang W, Du X, Tang Q, Li S, Odeh Z, Wu T, et al. (2017). Novel Mechanism of the Pericyte-Myofibroblast Transition in Renal Interstitial Fibrosis: Core Fucosylation Regulation. Sci Rep 7, 16914. [PubMed: 29209018]

Willis BC, duBois RM, and Borok Z. (2006). Epithelial origin of myofibroblasts during fibrosis in the lung. Proc Am Thorac Soc 3, 377–382. [PubMed: 16738204]

Wu CF, Chiang WC, Lai CF, Chang FC, Chen YT, Chou YH, Wu TH, Linn GR, Ling H, Wu KD, et al. (2013). Transforming growth factor beta-1 stimulates profibrotic epithelial signaling

to activate pericyte-myofibroblast transition in obstructive kidney fibrosis. Am J Pathol 182, 118–131. [PubMed: 23142380]

Wynn TA (2007). Common and unique mechanisms regulate fibrosis in various fibroproliferative diseases. J Clin Invest 117, 524–529. [PubMed: 17332879]

Xiao L, Zhou D, Tan RJ, Fu H, Zhou L, Hou FF, and Liu Y. (2016). Sustained Activation of Wnt/beta-Catenin Signaling Drives AKI to CKD Progression. Journal of the American Society of Nephrology : JASN 27, 1727–1740. [PubMed: 26453613]

Yan S, Zhou C, Zhang W, Zhang G, Zhao X, Yang S, Wang Y, Lu N, Zhu H, and Xu N. (2008). beta-Catenin/TCF pathway upregulates STAT3 expression in human esophageal squamous cell carcinoma. Cancer Lett 271, 85–97. [PubMed: 18602747]

Young S, Struys E, and Wood T. (2007). Quantification of creatine and guanidinoacetate using GC-MS and LC-MS/MS for the detection of cerebral creatine deficiency syndromes. Curr Protoc Hum Genet *Chapter 17*, Unit 17 13.

Yu H, Pardoll D, and Jove R. (2009). STATs in cancer inflammation and immunity: a leading role for STAT3. Nat Rev Cancer 9, 798–809. [PubMed: 19851315]

Zehender A, Huang J, Gyorfi AH, Matei AE, Trinh-Minh T, Xu X, Li YN, Chen CW, Lin J, Dees C, et al. (2018). The tyrosine phosphatase SHP2 controls TGFbeta-induced STAT3 signaling to regulate fibroblast activation and fibrosis. Nature communications 9, 3259.

Zeisberg EM, Tarnavski O, Zeisberg M, Dorfman AL, McMullen JR, Gustafsson E, Chandraker A, Yuan X, Pu WT, Roberts AB, et al. (2007). Endothelial-to-mesenchymal transition contributes to cardiac fibrosis. Nat Med 13, 952–961. [PubMed: 17660828]

Zhang F, Li C, Halfter H, and Liu J. (2003). Delineating an oncostatin M-activated STAT3 signaling pathway that coordinates the expression of genes involved in cell cycle regulation and extracellular matrix deposition of MCF-7 cells. Oncogene 22, 894–905. [PubMed: 12584569]

Zhang P, Cai Y, Soofi A, and Dressler GR (2012). Activation of Wnt11 by transforming growth factor-beta drives mesenchymal gene expression through non-canonical Wnt protein signaling in renal epithelial cells. J Biol Chem 287, 21290–21302. [PubMed: 22556418]

Zhou D, Tan RJ, Zhou L, Li Y, and Liu Y. (2013). Kidney tubular beta-catenin signaling controls interstitial fibroblast fate via epithelial-mesenchymal communication. Sci Rep 3, 1878. [PubMed: 23698793]

Zhou L, Li Y, Hao S, Zhou D, Tan RJ, Nie J, Hou FF, Kahn M, and Liu Y. (2015). Multiple genes of the renin-angiotensin system are novel targets of Wnt/beta-catenin signaling. Journal of the American Society of Nephrology : JASN 26, 107–120. [PubMed: 25012166]

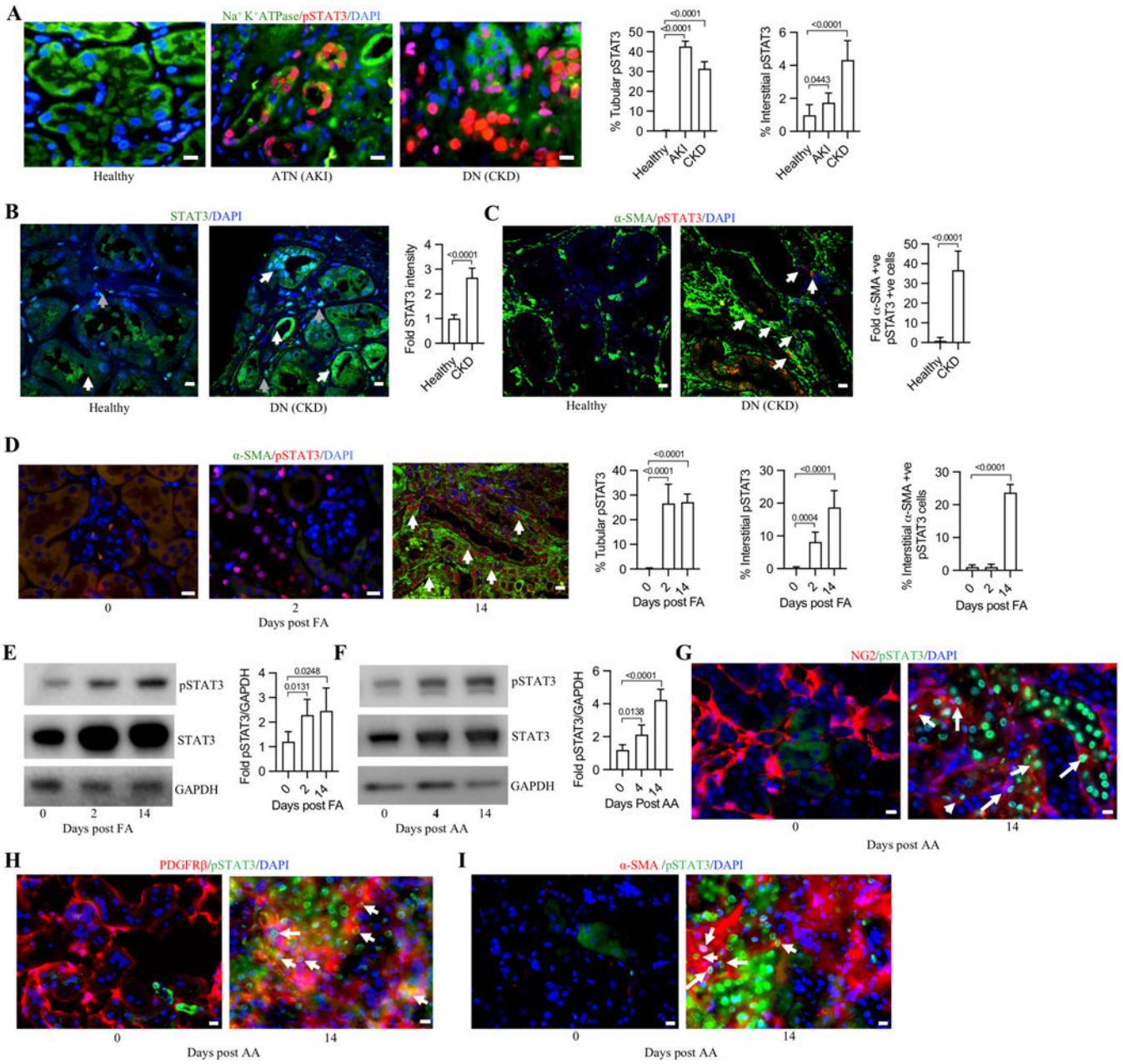

Figure 1. STAT3 is expressed in tubular epithelial cells in AKI and also in interstitial cells in CKD of human and mouse kidneys

(A) pSTAT3 immunostaining (red) in healthy (n=10), AKI (Acute Tubular Necrosis (ATN), n=5), and CKD (Diabetic Nephropathy (DN), n=10) paraffin sections of human kidneys. Na^+ K^+ ATPase (green) for tubular staining. DAPI staining (blue) for nuclei. Images were captured on a confocal microscope using 60X objective. Scale bar=10μm. Percentage of pSTAT3-positive tubular epithelial cells normalized to total nuclei (n=5–10). Percentage of pSTAT3-positive interstitial cells normalized to total nuclei (n=5–10). p-values are shown above the bars as determined by two-tailed unpaired T-Test.

(B) STAT3 immunostaining (green) in healthy and CKD paraffin sections of human kidneys (n=10). Images were captured on a confocal microscope using 60X objective. Scale bar=10

μm. White arrows show tubular and gray arrow show interstitial staining. Scale bar=10μm. Fold STAT3 intensity as compared to healthy kidneys plotted after normalization to number of total nuclei (n=10). p-values are shown above the bars as determined by two-tailed unpaired T-Test.

(C) Co-immunostaining for α-SMA (green) and pSTAT3 (red) staining on paraffin sections of human healthy and CKD kidneys (n=10). Arrows show double-positive cells. Scale bar=10μm. Images were captured on a confocal microscope using 60X objective. Fold of α-SMA and pSTAT3 double-positive cells were plotted as compared to healthy kidneys (n=10). p-values are shown above the bars as determined by two-tailed unpaired T-Test.

(D) α-SMA (green) and pSTAT3 (red) in normal (day 0) and folic acid-induced AKI (day 2) and fibrotic (day 14) paraffin kidney sections. Double-positive cells are shown by arrows (n=5). Scale bar=10μm. Quantitation of percentage of tubular pSTAT3-positive cells normalized to total nuclei (n=5). Quantitation of percentage of interstitial pSTAT3-positive cells normalized to total nuclei (n=5). Quantitation of percentage of α-SMA and pSTAT3-positive cells (n=5). p-values are shown above the bars as determined by two-tailed unpaired T-Test.

(E) Western blotting for pSTAT3 and STAT3 in normal (day 0) kidneys and folic acid (FA)-induced AKI (day 2) and fibrotic (day 14) kidneys. Quantitation of fold change in pSTAT3 compared to normal kidneys and normalized to GAPDH loading control (n=5). p-values are shown above the bars as determined by two-tailed unpaired T-Test.

(F) Western blotting for pSTAT3 and STAT3 in normal (day 0) kidneys and aristolochic acid (AA)-induced AKI (day 4) and fibrotic (day 14) kidneys. Quantitation of fold change in pSTAT3 compared to normal kidneys and normalized to GAPDH (n=5). p-values are shown above the bars as determined by two-tailed unpaired T-Test.

(G-I) Co-immunostaining for pSTAT3 (green) and NG2 (red) or PDGFRβ (red) or α-SMA (red) respectively, in mouse OCT kidney sections 14-days post-AA treatment (n=5). White arrow indicates double-positive cells. Scale bar=10μm. Images were captured on a wide field microscope using 60X objective.

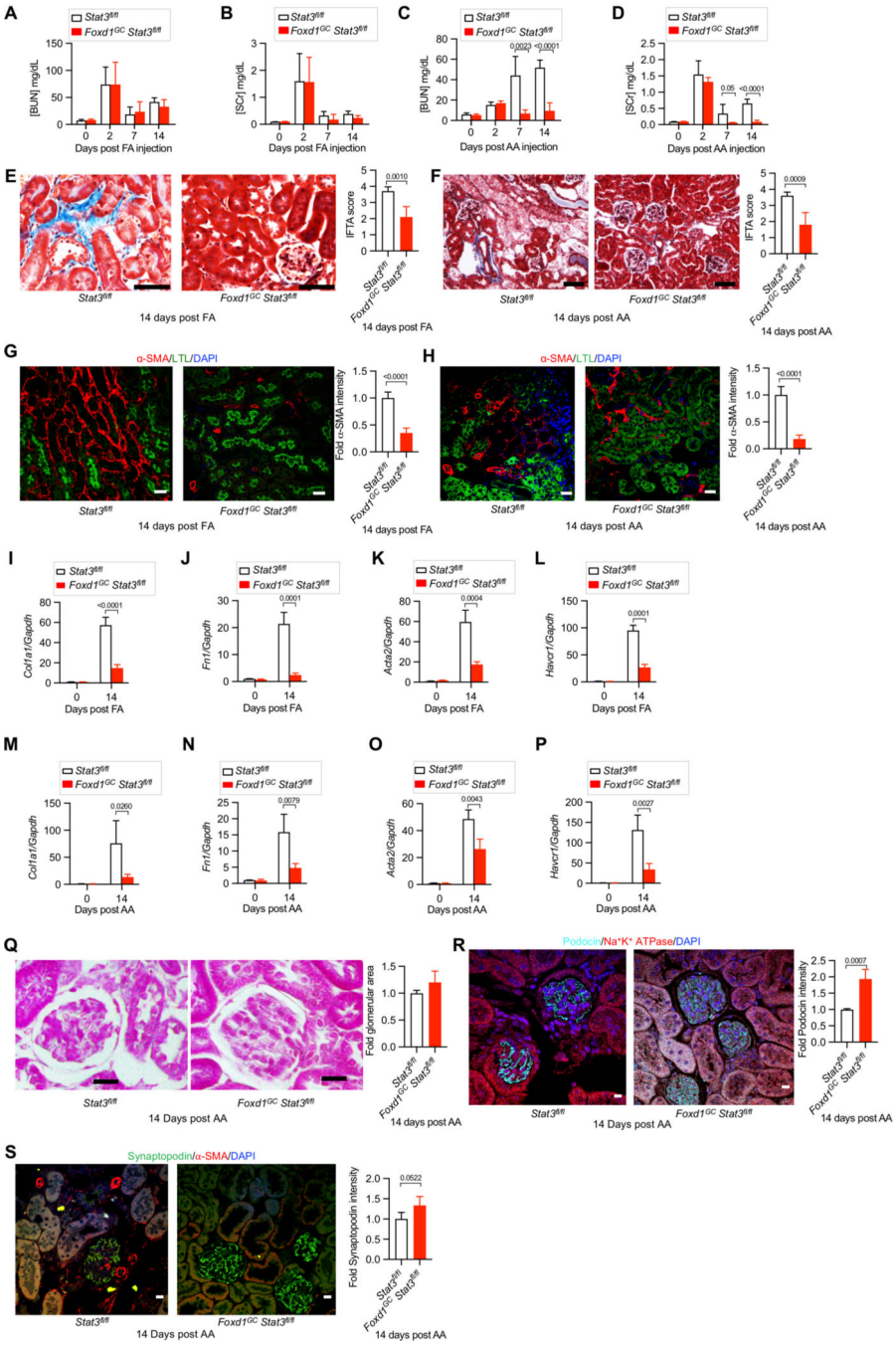

Figure 2. Foxd1 Cre-mediated depletion of *Stat3* protects mice from folic acid and aristolochic acid-induced kidney fibrosis

(A-D) BUN and sCr estimation for kidney dysfunction in FA- (A and B) or AA- (C and D) induced kidney injury in control (*Stat3*$^{fl/fl}$) and *Stat3* KO (*Foxd1*^{GC} *Stat3*$^{fl/fl}$) mice, 14-days post-treatment (n=5). p-values are shown above the bars as determined by two-tailed unpaired T-Test.

(E and F) Masson Trichrome Staining (MTS) and Interstitial Fibrosis and Tubular Atrophy (IFTA) scoring following 14-days post-FA- (E) or AA- (F) treatment in control and *Stat3* KO mouse kidneys (n=5). Scale bar=10μm. Average IFTA scores were plotted for normal

and Stat3 KO mice, 14-days post-FA- or AA-treatment (n=5). p-values are shown above the bars as determined by two-tailed unpaired T-Test.

(G and H) Co-immunostaining for LTL (green) and α-SMA (red) and its quantitation in kidneys at 14-days post-FA- (G) or AA- (H) induced kidney fibrosis in control and *Stat3* KO mice. Scale bar=10 μm. Images were captured on a confocal microscope using 60X objective. Fold change in intensity for α-SMA normalized to cell number were plotted in comparison to control mice. p-values are shown above the bars as determined by two-tailed unpaired T-Test.

(I-P) TaqMan based gene expression analysis for *Col1a1*, *Fn1*, *Acta2,* and *Havcr1* at 14-days post-treatment with FA (I-L) or AA (M-P) for control and *Stat3* KO mouse kidneys (n=4). Fold changes were plotted in comparison to control mice at day 0. p-values are shown above the bars as determined by two-tailed unpaired T-Test.

(Q) Representative histology on PAS stain focusing on glomerulus from 14-days post-AA treated control and *Stat3* KO mice. Scale bar=10μm. Fold of average glomerular size in comparison to control mice (n=4 mice). p-values are shown above the bars as determined by two-tailed unpaired T-Test.

(R) Co-immunostaining for podocin (green) and Na^+ K^+ ATPase (red) on kidney paraffin sections of 14-days post-AA treated control and *Stat3* KO mice. Scale bar=10μm. Images were captured on a confocal microscope using 60X objective. Fold change in the podocin intensity normalized to number of glomeruli in comparison to control mice (n=5). p-values are shown above the bars as determined by two-tailed unpaired T-Test.

(S) Co-immunostaining for synaptopodin (green) and α-SMA (red) on kidney paraffin sections of 14-days post-AA treated control and *Stat3* KO mice. Scale bar=10μm. Images were captured on a confocal microscope using 60X objective. Fold change in synaptopodin intensity normalized to number of glomeruli in comparison to control mice (n=5). p-values are shown above the bars as determined by two-tailed unpaired T-Test.

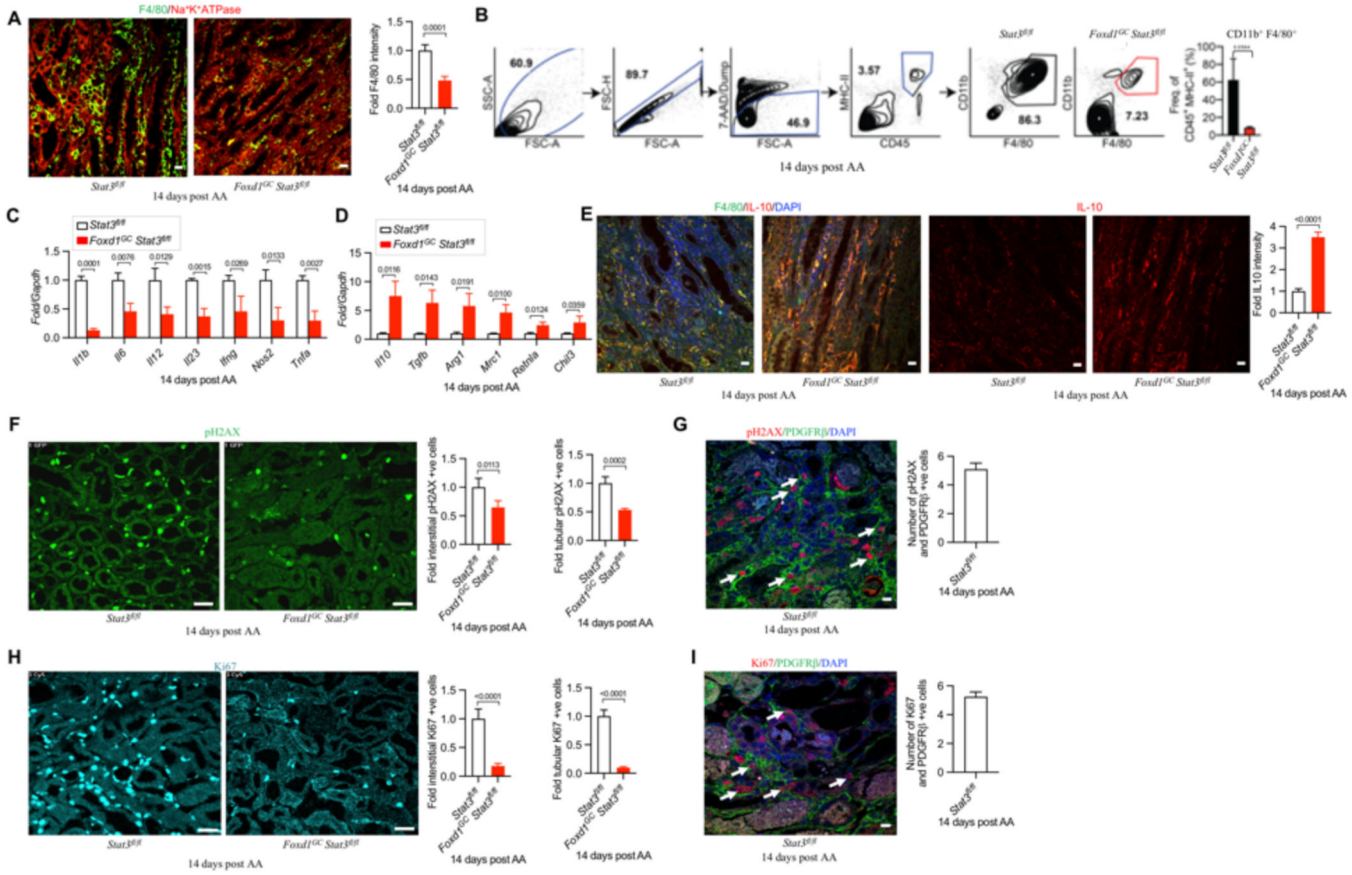

Figure 3. Foxd1 Cre-mediated depletion of *Stat3* shows decreased macrophage infiltration, inflammation, decreased DNA damage signaling, and reduced cell proliferation in fibrotic kidneys

(A) Co-immunostaining for F4/80 (green) and Na^+ K^+ ATPase (red) on the paraffin sections of mouse kidneys at 14-days post-AA treatment. Scale bar=10μm. Fold change in the intensity of F4/80 normalized to nuclei and plotted in comparison to control kidneys at day 14 post-AA treatment (n=4). p-values are shown above the bars as determined by two-tailed unpaired T-Test.

(B) FACS sorting strategy for macrophages from control and *Stat3* KO mouse kidneys at 14-days post-AA treatment.

TaqMan base quantitative RT-PCR for (C) inflammatory mediators/M1 markers and (D) M2 markers from macrophages isolated from mouse kidneys at 14-days post-AA treatment. Fold changes were plotted in comparison to control mice at 14-days post-AA treatment (n=3). p-values are shown above the bars as determined by two-tailed unpaired T-Test.

(E) Co-immunostaining of F4/80 (green) and IL-10 (red) and IL-10 (red) alone on the paraffin sections of mouse kidneys 14-days post-AA treatment. Scale bar=10μm. Fold change in the intensity of IL-10 normalized to nuclei and plotted in comparison to control kidneys at day-14 post-AA treatment (n=4). p-values are shown above the bars as determined by two-tailed unpaired T-Test.

(F) Representative immunostaining for pH2AX (green) in the control and *Stat3* KO mouse paraffin kidney sections at 14-days post-AA injection. Scale bar=10μm. Images were

captured on a widefield immunofluorescence microscope using 60X objective. Quantitation of interstitial and tubular pH2AX positive cells (n=4). Fold changes were calculated by normalizing the number of pH2AX cells to number of nuclei and plotted in comparison to control mice at 14-days post-AA treatment. p-values are shown above the bars as determined by two-tailed unpaired T-Test.

(G) Co-immunostaining for PDGFRβ (green) and pH2AX (red) on the paraffin sections of control mouse kidneys at 14-days post-AA treatment. Scale bar=10μm. PDGFRβ and pH2AX double-positive cells are shown by white arrows. Number of PDGFRβ and pH2AX double-positive cells were counted and plotted (n=4).

(H) Immunostaining for Ki67 (cyan) in the mouse kidneys 14-days post-AA injection. Images were captured on a widefield immunofluorescence microscope using 60X objective. Quantitation of interstitial and tubular Ki67 positive cells (n=4). Scale bar=10μm. Fold changes were calculated by normalizing the number of pH2AX cells to number of nuclei and plotted in comparison to control mice at 14-days post-AA treatment. p-values are shown above the bars as determined by two-tailed unpaired T-Test.

(I) Co-immunostaining for PDGFRβ (green) and Ki67 (red) on the paraffin sections of control mouse kidneys at 14-days post-AA treatment. Scale bar=10μm. PDGFRβ and Ki67 double-positive cells are shown by white arrows. Number of PDGFRβ and Ki67 double-positive cells were counted and plotted (n=4).

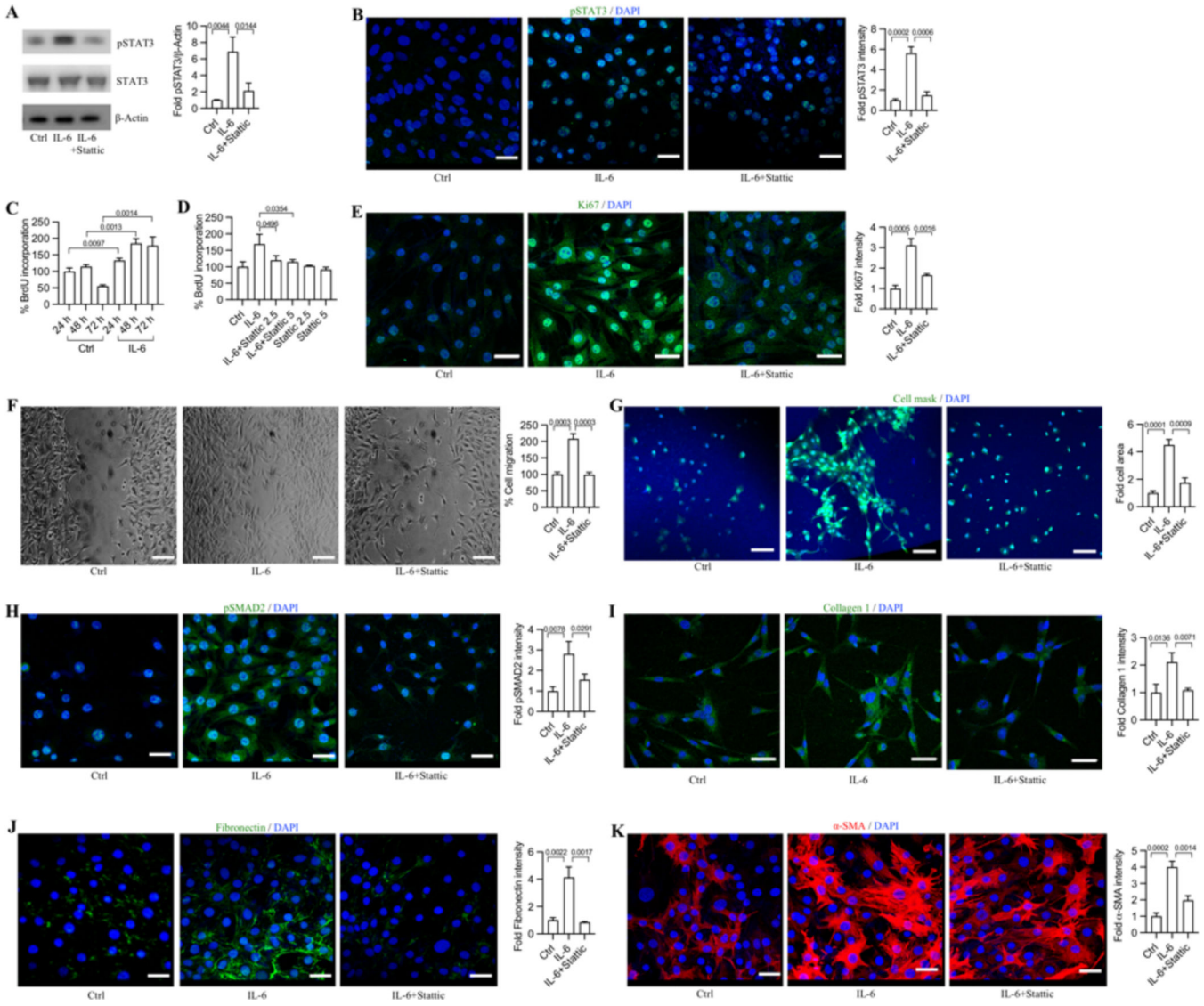

Figure 4. IL-6-mediated STAT3 phosphorylation regulates proliferation, migration, and profibrotic signaling in pericyte-like 10T1/2 cells

(A) Representative western blots for pSTAT3 and STAT3 following treatment with IL-6 or IL-6 in combination with stattic in 10T1/2 cells. Fold changes were calculated after normalization to b-Actin and plotted in comparison to control (ctrl) cells (n = 3). p-values are shown above the bars as determined by two-tailed unpaired T-Test.

(B) Nuclear translocation of STAT3 in 10T1/2 cells following IL-6 and or stattic treatment. Scale bar=10μm. Intensity of pSTAT3 were normalized to total number of cells and fold change in comparison to control cells were plotted (n = 3). p-values are shown above the bars as determined by two-tailed unpaired T-Test.

Proliferation of 10T1/2 cells following IL-6 and stattic treatments using BrdU incorporation assay in a (C) time- and (D) STAT3-dependent manner (n=3). p-values are shown above the bars as determined by two-tailed unpaired T-Test.

(E) Immunofluorescence staining for Ki67 with or without IL-6 and stattic treatments in 10T1/2 cells. Scale bar=10μm. Intensity of Ki67 were normalized to total number of cells

and fold change in comparison to control cells were plotted (n=3). p-values are shown above the bars as determined by two-tailed unpaired T-Test.

(F) Migration of 10T1/2 cells following IL-6 and stattic treatment using scratch assay. Scale bar=50μm. Percent cell migration was calculated as compared to gap area in the control cells at 24 hours (n=3). p-values are shown above the bars as determined by two-tailed unpaired T-Test.

(G) Transwell migration of 10T1/2 cells treated with IL-6 or IL-6 in combination with stattic. Scale bar=50μm. Cell area normalized to cell number were calculated for CellMask stain (green) and fold change was calculated as compared to control cells (n=3). p-values are shown above the bars as determined by two-tailed unpaired T-Test.

(H-K) Immunostaining for (H) pSMAD2 (green), (I) Collagen 1 (green), (J) Fibronectin (green) and (K) α-SMA (green) following IL-6 alone or in combination with stattic on 10T1/2 cells. Scale bar=10μm. Intensity of pSMAD2, Collagen 1, Fibronectin, and α-SMA were normalized with number of cells and fold change were plotted in comparison to control cells (n=3). p-values are shown above the bars as determined by two-tailed unpaired T-Test.

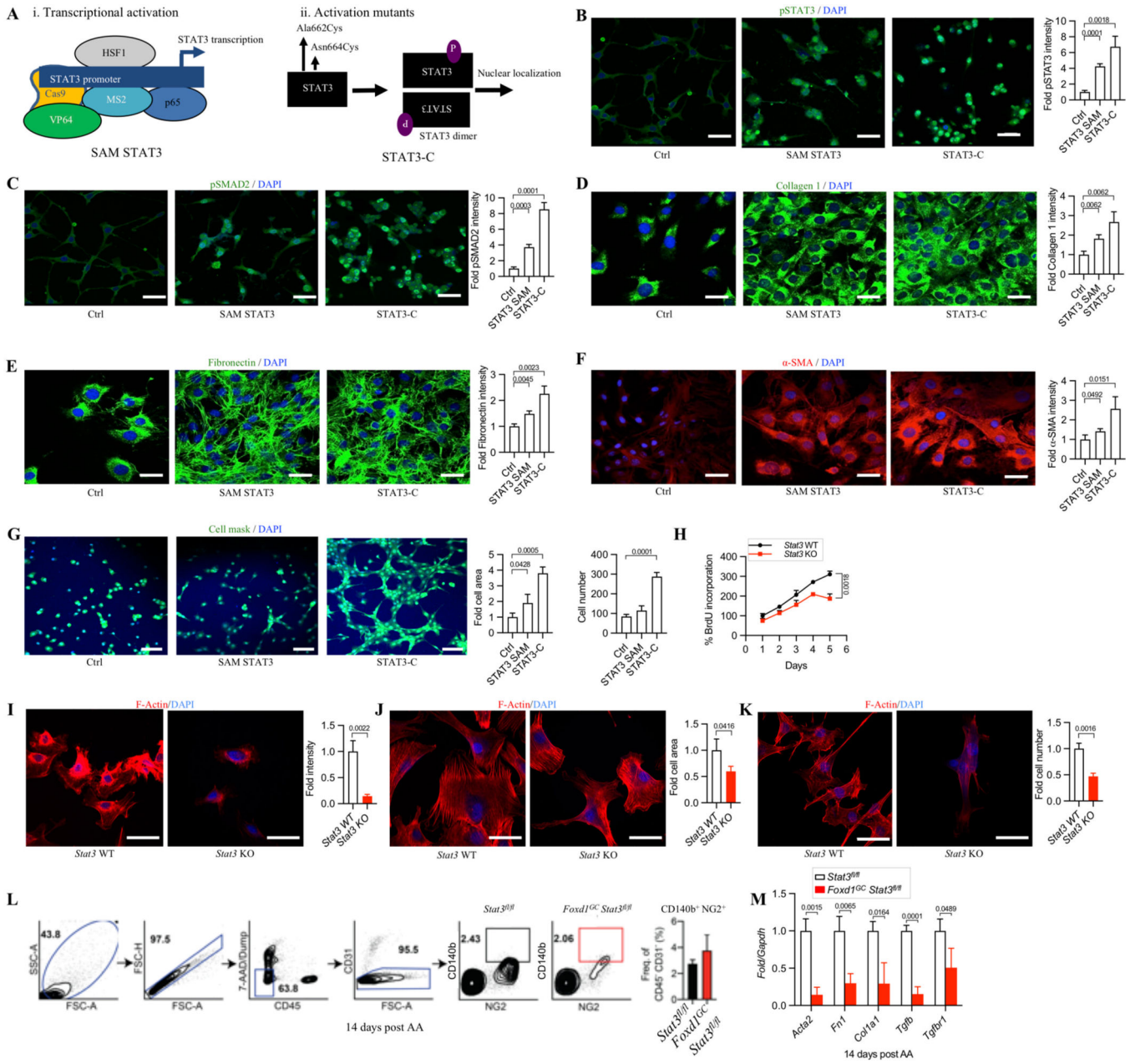

Figure 5. STAT3 directly regulates attachment, spreading, migration, proliferation, and profibrotic signaling in 10T1/2 cells

(A) Scheme for STAT3 activation using synergistic activation mediators (SAM) and activation mutants (STAT3-C).

(B-F) Immunostaining for (B) pSTAT3 (green), (C) pSMAD2 (green), (D) Collagen 1, (E) Fibronectin, and (F) α-SMA (green) on STAT3 activated 10T1/2 cells. Scale bar=10μm. Intensity of staining for pSTAT3, pSMAD2, Collagen 1, Fibronectin, and α-SMA were normalized with cell numbers and plotted in comparison to control (ctrl) cells (n=3). p-values are shown above the bars as determined by two-tailed unpaired T-Test.

(G) Transwell migration of 10T1/2 cells in STAT3-activated cells. Scale bar=50μm. Cell area normalized to cell number was calculated by CellMask and fold change was plotted in

comparison to control cells (n=3). Total number of migrated cells were counted on the lower side of the polycarbonate membrane by counting the nuclei (n=3). p-values are shown above the bars as determined by two-tailed unpaired T-Test.

(H) Proliferation of *Stat3* WT and KO 10T1/2 cells as assayed by BrdU incorporation assay for 5 days. Percent change was calculated in comparison to day-1 *Stat3* WT cells (n=3). p-values are shown above the bars as determined by two-tailed unpaired T-Test.

(I) Adherence assay as shown by staining for F-actin (red) of *Stat3* WT and *Stat3* KO 10T1/2 cells at 1-hour after plating. Scale bar=10μm. Intensity of F-actin normalized to total cell number were calculated and fold change were calculated in comparison to *Stat3* WT cells (n=3). p-values are shown above the bars as determined by two-tailed unpaired T-Test.

(J) Spreading assay as shown staining for F-actin (red) of *Stat3* WT and *Stat3* KO 10T1/2 cells at 3-hours after plating. Scale bar=10μm. Cell area of F-actin normalized to total cell number and fold change were calculated in comparison to *Stat3* WT cells (n=3). p-values are shown above the bars as determined by two-tailed unpaired T-Test.

(K) Transwell migration assay as shown by staining for F-actin (red). Scale bar=10μm. Total number of migrated cells were calculated by counting the DAPI on the lower side of the polycarbonate membrane and fold change was calculated in comparison to *Stat3* WT 10T1/2 cells. p-values are shown above the bars as determined by two-tailed unpaired T-Test.

(L) FACS sorting strategy for isolating pericytes from fibrotic mouse kidneys and its quantitation.

(M) TaqMan based quantitative RT-PCR for profibrotic factors in the pericytes isolated from control and *Stat3* KO mice at day-14 post-AA treatment (n=3). p-values are shown above the bars as determined by two-tailed unpaired T-Test.

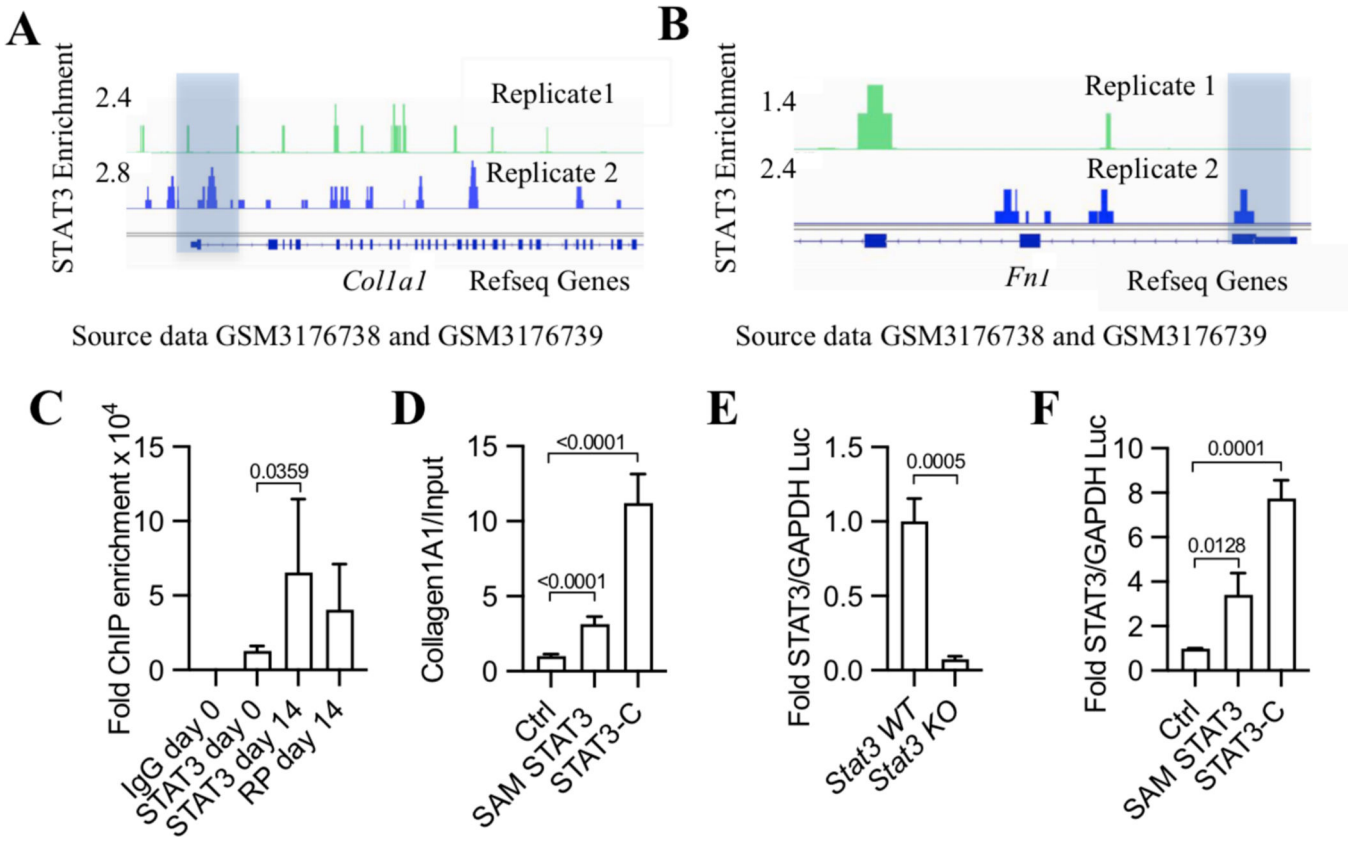

Figure 6. STAT3 binds *Collagen1a1* promoter in mouse kidneys and in pericytes cell line to induce profibrotic signaling

(A and B) Analysis of previously published STAT3 ChIP sequencing data showing STAT3 binding mouse *Collagen1a1* and *Fibronectin 1* promoter regions. Log of fold enrichment are plotted for each replicate (n=2).

(C) ChIP assay using anti-STAT3 antibody in normal and 14-days post-AA treatment in the mouse kidneys to detect STAT3 binding on *Collagen1a1* promoter. Fold enrichments were normalized to input and were plotted in comparison to IgG at day 0 samples (n=3). Rabbit IgG and RNA polymerase (RP) antibodies are negative and positive controls. p-values are shown above the bars as determined by two-tailed unpaired T-Test.

(D) ChIP assay using anti-STAT3 antibody in 10T1/2 cells with activated STAT3 to detect STAT3 binding on *Collagen1a1* promoter. Fold enrichments were normalized to input and fold change were plotted in comparison to control cells (n=5). p-values are shown above the bars as determined by two-tailed unpaired T-Test.

(E and F) Luciferase assay to detect STAT3 binding on *STAT3* consensus sequence in (E) *Stat3* KO and (F) STAT3-activated 10T1/2 cells. RLU values of firefly luciferase (*STAT3* luciferase) was normalized to renilla luciferase (*GAPDH* luciferase) and fold changes were calculated in comparison to *Stat3* WT or Ctrl cells in Figures 6E and 6F respectively. p-values are shown above the bars as determined by two-tailed unpaired T-Test.

KEY RESOURCES TABLE

Primary and secondary antibodies

Antibodies	Vendor	Clone	Cat. number
Anti-CD3e-PerCP	Biolegend	145–2C11	100326
Anti-NK1.1-PerCP	Biolegend	PK136	108726
Anti-CD19-PerCP	Biolegend	6D5	115532
Anti-CD45-FITC	Biolegend	30-F11	103108
Anti-CD11b-PE	Biolegend	M1/70	101208
Anti-MHC-II-APC-Cy7	Biolegend	M5/114.152	107628
Anti-F4/80-PE-Cy7	Biolegend	BM8	123114
Anti-CD45-PE-Cy7	Biolegend	30-F11	103114
Anti-CD31-PE	Biolegend	390	102407
Anti-CD140b-APC	Biolegend	APB5	136007
Anti-NG2-AF488	EMD Millipore	N/A	AB5320A4
7AAD viability solution	Biolegend	N/A	420404
Anti-pSTAT3	Cell Signaling	D3A7	9145
Anti-STAT3	Cell Signaling	124H6	9139
Anti-Ki67	Cell Signaling	8D5	9449
Anti-BrdU	Cell Signaling	Bu20a	5292
Anti-Fibronectin	Abcam	N/A	ab2413
Anti-Collagen1	Abcam	N/A	ab34710
Anti-alpha Smooth Muscle Actin	Millipore Sigma	1A4	A5228
Anti-SMAD2	Cell Signaling	D43B4	5339
Anti-Na^+ K^+ ATPase	Abcam	EP1845Y	ab76020
Anti-PDGFR beta	Abcam	Y92	ab32570
Anti-F4/80	Cell Signaling	D4C8V	30325
Anti-pH2AX	Cell Signaling	20E3	9718
Anti-NG2	Millipore Sigma	132.38	MAB5384-I-100UG
Anti-GAPDH	Millipore Sigma	N/A	SAB2108668–100UL
Anti-IL-10	R&D Systems	948505	MAB9184–100
Anti-Synaptopodin	Santa Cruz Biotechnology	D-9	sc-515842
Anti-Podocin	Novus Biologicals	JB51–33	NBP2–75624
Anti-Rabbit conjugated HRP	Cell Signaling	N/A	7074
Anti-Mouse conjugated HRP	Cell Signaling	N/A	7076
Alexa Flour 488 conjugated Goat anti-Rabbit IgG	Thermo Fisher Scientific	N/A	A32731
Alexa Flour 488 conjugated Goat anti-Rat IgG	Invitrogen	N/A	A-11006
Alexa Flour 488 conjugated Goat anti-Mouse IgG	Invitrogen	N/A	A-32723
Alexa Flour 594 conjugated Goat anti-Rabbit IgG	Invitrogen	N/A	A-11037
Alexa Flour 647 conjugated Goat anti-Rabbit IgG	Invitrogen	N/A	A-32733

Antibodies	Vendor	Clone	Cat. number
Alexa Flour 594 conjugated Goat anti-Mouse IgG	Invitrogen	N/A	A-11005

Chemicals and recombinant proteins

Chemicals and proteins	Vendor	Cat. number
Stattic	Millipore Sigma	R415
IL-6	R&D Systems	7270-IL-025/CF
DAPI	Vector laboratories	H-1200–10
F-Actin	Invitrogen	A-12381
Cell mask	Thermo Fisher Scientific	C2925
Eagle's Basal medium	Thermo Fisher Scientific	21010–046
BrdU	Thermo Fisher Scientific	B5002–5G
Heparin	Fisher Scientific	H19
LTL	Vector Laboratories	NC0127927
Dual luciferase assay kit	Promega Corporation	E1910
Glutamine	ATCC	30–2214
Lightning-Link® Rapid Alexa Fluor 488 Antibody Labeling Kit	Novus Biologicals	ab236553

Mouse

Mouse	Source	Stock number
Stat3^{tm1Xyfu} */J (Stat3*^{flox}*)*	The Jackson Laboratory	016923
Foxd1$^{GFP\text{-}Cre}$*(Foxd1*^{GC}*)*	(Kobayashi et al., 2014)	N/A

Software

Name	Vendor	Identification number
GraphPad Prism 9	GraphPad Software	RRID:SCR_002798
FIJI v1.0	(Schindelin et al., 2012)	RRID:SCR_003070
FlowJo 10.6.2	FlowJo	RRID:SCR_008520; https://www.flowjo.com/